# Platform Reagents Enable Synthesis of Ligand-Directed Covalent Probes: Study of Cannabinoid Receptor 2 in Live Cells

Miroslav Kosar,[a] David A. Sykes,[b] Alexander E. G. Viray,[c] Rosa Maria Vitale,[d] Roman C. Sarott,[a] Rudolf L. Ganzoni,[a] David Onion,[e] Janelle M. Tobias,[c] Philipp Leippe,[f] Christoph Ullmer,[g] Elisabeth A. Zirwes,[g] Wolfgang Guba,[g] Uwe Grether,*[g] James A. Frank,*[c,h] Dmitry B. Veprintsev,*[b] and Erick M. Carreira*[a]

[a]Laboratorium für Organische Chemie, Eidgenössische Technische Hochschule Zürich, Vladimir-Prelog-Weg 3, 8093 Zürich, Switzerland
[b]Centre of Membrane Proteins and Receptors (COMPARE), University of Birmingham and University of Nottingham, Midlands, UK; Faculty of Medicine & Health Sciences, University of Nottingham, Nottingham NG7 2UH, UK
[c] Department of Chemical Physiology & Biochemistry, Oregon Health & Science University, Portland, Oregon 97239-3098, United States
[d]Institute of Biomolecular Chemistry, National Research Council (ICB-CNR), Via Campi Flegrei 34, 80078 Pozzuoli, Italy
[e]School of Life Sciences, University of Nottingham, Nottingham NG7 2UH, UK
[f]Department of Chemical Biology, Max Planck Institute for Medical Research, Jahnstr. 29, 69120 Heidelberg, Germany
[g]Roche Pharma Research & Early Development, Roche Innovation Center Basel, F. Hoffmann-La Roche Ltd., 4070 Basel, Switzerland
[h]Vollum Institute, Oregon Health & Science University, Portland, Oregon 97239-3098, United States

*Ligand-directed covalent labeling • TR-FRET • Fluorogenic • G protein-coupled receptors • Cannabinoid type 2 receptor ($CB_2R$)*

**ABSTRACT:** Pharmacological modulation of cannabinoid receptor type 2 ($CB_2R$) holds promise for the treatment of neuroinflammatory disorders, such as Alzheimer's disease. Despite the importance of $CB_2R$, its expression and downstream signaling are insufficiently understood in disease- and tissue-specific contexts. Herein, we report the first ligand-directed covalent (LDC) labeling of $CB_2R$ enabled by a novel synthetic strategy and application of platform reagents. The LDC modification allows visualization and study of $CB_2R$ while maintaining its ability to bind other ligands at the orthosteric site. We employed *in silico* docking and molecular dynamics simulations to guide probe design and assess feasibility of LDC labeling of $CB_2R$. We demonstrate selective, covalent labeling of a peripheral lysine residue of $CB_2R$ by exploiting fluorogenic *O*-nitrobenzoxadiazole (*O*-NBD) functionalized probes in a TR-FRET assay. The rapid proof-of-concept validation with *O*-NBD probes inspired incorporation of advanced electrophiles suitable for experiments in live cells. To this end, novel synthetic strategies toward *N*-sulfonyl pyridone and *N*-acyl-*N*-alkyl sulfonamide LDC probes were developed, which allowed covalent delivery of fluorophores suitable for cellular studies. The LDC probes were characterized by a radioligand binding assay and TR-FRET experiments. Additionally, the probes were applied to specifically visualize $CB_2R$ in conventional and imaging flow cytometry as well as in confocal fluorescence microscopy using overexpressing and endogenously expressing microglial live cells.

## INTRODUCTION

Cannabinoid receptors type 1 and 2 ($CB_1R$ and $CB_2R$) are essential components of the endocannabinoid system (eCBS), which is of fundamental importance in a wide range of physiological processes in all vertebrates.[1,2] $CB_1R$ is most abundant in the central nervous system, whereas $CB_2R$ is expressed predominantly at the periphery by cells of the immune system.[3-5] Dysregulation of the eCBS, specifically of $CB_2R$ signaling, has been implicated in numerous diseases including tissue injury, inflammation,[6,7] and neurodegenerative conditions.[8,9] Despite early studies suggesting expression of $CB_2R$ exclusively restricted to the periphery,[3,10,11] there is mounting evidence that $CB_2R$ is expressed also in the brain.[12-16] Notably, brain glial cells, which play a crucial role in modulating immune response,[17] were found to express $CB_2R$.[18,19] Additionally, their significance was established in ameliorating neuroinflammatory diseases.[20,21]

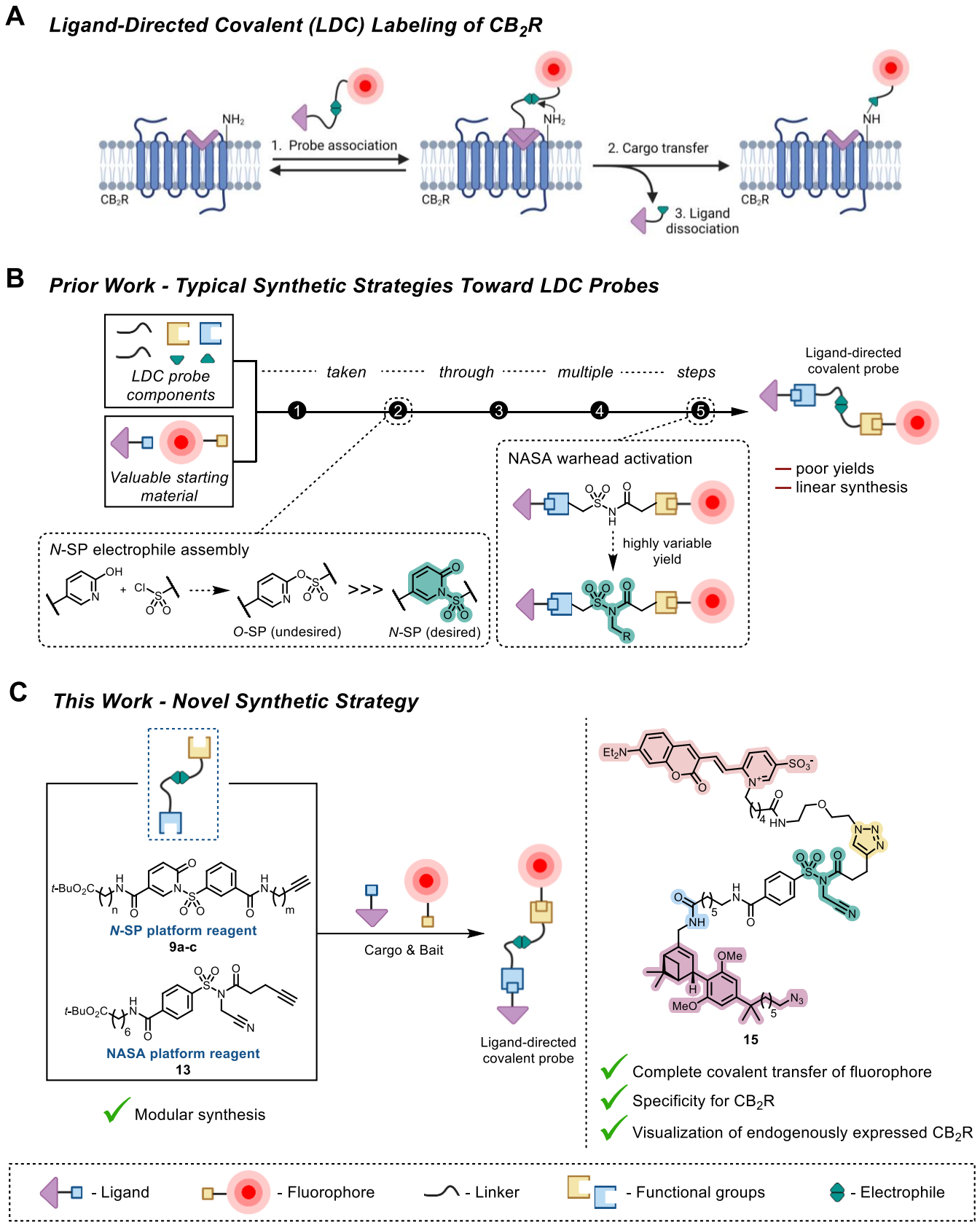


**Figure 1. A** Ligand-directed covalent (LDC) labeling of $CB_2R$. The process commences with affinity-driven association of the LDC probe with the receptor (1.), followed by proximity-driven covalent cargo transfer (2.) with subsequent dissociation of ligand from receptor (3.). **B** Comparison of typical prior strategies toward LDC probes using a linear functionalization of either ligand or fluorophore. **C** Herein reported work using a modular assembly with *N*-sulfonyl pyridone (*N*-SP) **9a-c** and *N*-acyl-*N*-alkyl sulfonamide (NASA) **13** platform reagents.[22]

Expression of $CB_2R$ is significantly upregulated under pathological conditions,[23,24] however, despite its evident importance, no therapeutics targeting the receptor selectively have been brought to the market. This shortcoming is largely attributed to poor understanding of receptor biology, in particular, its expression in tissue- and disease–dependent contexts. The situation is further complicated by the lack of specific antibodies,[25-28] scarcity of validated chemical probes,[29,30] and very low expression levels in native cells.[31-33]

Fluorescent probes have emerged as a powerful tool enabling the study of ligand-protein interactions with unrivaled spatiotemporal resolution.[34] Recently, our group has reported a potent $CB_2R$ selective agonist scaffold, which was functionalized with a variety of fluorophores to enable visualization of $CB_2R$.[30,35] However, these probes are inherently limited in the study of native receptor biology, since they occupy the orthosteric ligand binding site. As such, they continuously exert their strong agonistic effects, which lead to disruption of cellular homeostasis and internalization of membrane-bound receptors.[33] Importantly, the fluorescent probe precludes binding by the respective endogenous ligands, perturbing the native state of $CB_2R$ and associated downstream signaling. We surmised that these limitations could be addressed by introduction of cleavable, reactive motifs within the probe that transfer a fluorophore to the periphery of the protein of interest in a ligand-directed manner (Figure 1A). This strategy of affinity labeling, known as ligand-directed covalent (LDC) chemistry, allows for highly specific, fluorescent tagging of endogenously expressed proteins in complex, multimolecular systems.[36-38] The LDC process commences with nucleophilic attack by a proximal amino acid residue at the surface of the receptor. Following peripheral, covalent labeling, the ligand is free to dissociate from the binding site, and the native function of the receptor is preserved.[39,40] This technique has been successfully applied to label both intracellular and membrane bound protein targets *in vitro*, in cells,[41-49] in brain slices,[39,40,50] and even in animals.[51]

In our continuing investigation of the eCBS, we recently became interested in developing LDC probes for $CB_2R$, for which no precedent is available. In this respect, we were inspired by the work of Hamachi, who has reported the use of *N*-sulfonyl pyridone[52] (*N*-SP) and *N*-acyl-*N*-alkyl sulfonamide[53] (NASA) motifs in LDC chemistry. Valuable ligands and fluorophores, which themselves may require challenging synthetic efforts, are frequently the starting materials for the reported syntheses of LDC probes (Figure 1B). Additionally, during formation of the *N*-SP electrophile an undesired *O*-SP constitutional isomer is formed preferentially leading to a reduced yield. The starting materials are subjected to a long linear synthesis (up to 6-steps) and thus fall prey to the synthetic "arithmetic demon",[54] or diminution in material throughput incurred by a multi-step sequence.[55] Consequently, investigations of new protein targets often necessitate preparation of multiple probes and hence may be restricted to ligands or fluorophores available in sufficient quantities (grams), either from commercial sources or synthetic work.

We set out to devise new synthetic platforms for convergent and modular access toward LDC probes to enable broader applications and, specifically, for our studies of $CB_2R$ in live cells (Figure 1C). The new approach enabled design and synthesis of *N*-SP and NASA platform reagents **9a-c** and **13**, which conveniently allow rapid assembly of LDC probes for $CB_2R$. Remarkably, the *N*-SP and NASA platform reagents we report can be coupled to free primary amines, despite the fact that these incorporate reactive electrophilic sites designed to trap *N*ε of lysine. We successfully demonstrate the suitability of our LDC probes to study $CB_2R$ in live cells by flow cytometry, imaging flow cytometry, and fluorescence confocal microscopy in endogenously expressing cells. More broadly, the availability of the *N*-SP **9a-c** and NASA **13** platform reagents expands the targetable proteome and deliverable functionalities of LDC approaches by introduction of diverse bait and cargo elements late in the synthetic sequence.

## RESULTS AND DISCUSSION

### *O*-Nitrobenzoxadiazole: Rapid Proof-of-Concept by Fluorogenic Covalent Delivery

In general, an LDC probe consists of four components: high-affinity ligand, linker, reporter element and electrophilic motif, which can deliver the reporter and simultaneously release the ligand.[56,57] There are multiple challenges to the successful design of affinity labeling probes. A pitfall to be avoided is the introduction of a reporter element that adversely influences selectivity bias over closely related targets[58] or triggers significant decrease in affinity in comparison to the parent ligand.[59-61] Retention of high binding affinity is paramount as it may directly influence the rate of covalent cargo transfer.[53]

We have previously established the primary amine in **1a** as an optimal locus for linking ligand **1a** to a wide range of fluorophores (Scheme 1).[30,35] We opted to append agonist **1a** to an electrophilic motif subject to cleavage following ligand binding to the orthosteric site and reaction with a nearby lysine. Generally, selective modification of surface lysine residues is particularly challenging due to the high degree of solvation and low nucleophilicity.[62] Accordingly, we set out to investigate whether any lysine residues peripheral to the $CB_2R$ binding site are amenable to covalent modification.

In practice, we were attracted to *O*-linked nitrobenzoxadiazoles (NBD) **Ia-e** as they combine electrophile and reporter in a single motif. A key feature of **Ia-e** is that the alkyl *O*-linked NBDs are non-fluorescent, whereas *N*-linked NBDs formed upon reaction with alkyl amines (lysine residues) exhibit dramatic increase in fluorescence intensity.[63-65] This combination of electrophilic reactivity (via $S_NAr$) with fluorogenicity was seen as ideal to rapidly evaluate covalent modification. Furthermore, the small NBD unit combined with the distal nature of labeling site was expected to exert minimal impact on the endogenous activity of $CB_2R$.

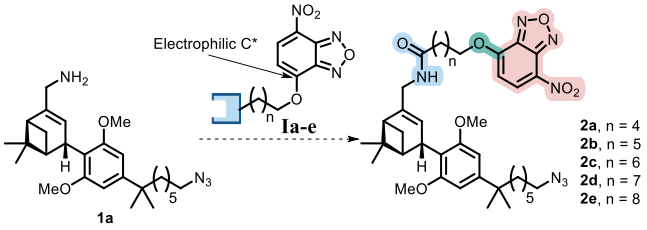


**Scheme 1.** Design of LDC *O*-NBD probes targeting $CB_2R$.

### *In Silico* Probe Design & Molecular Dynamics Simulation

Examination of the cryo-EM structure of $CB_2R$ with agonist WIN 55,212-2 (PDB:6PT0) revealed two lysines, namely $Lys23^{NTER}$ and $Lys103^{3.22}$ on the surface of $CB_2R$ in proximity to the orthosteric binding site.[66]

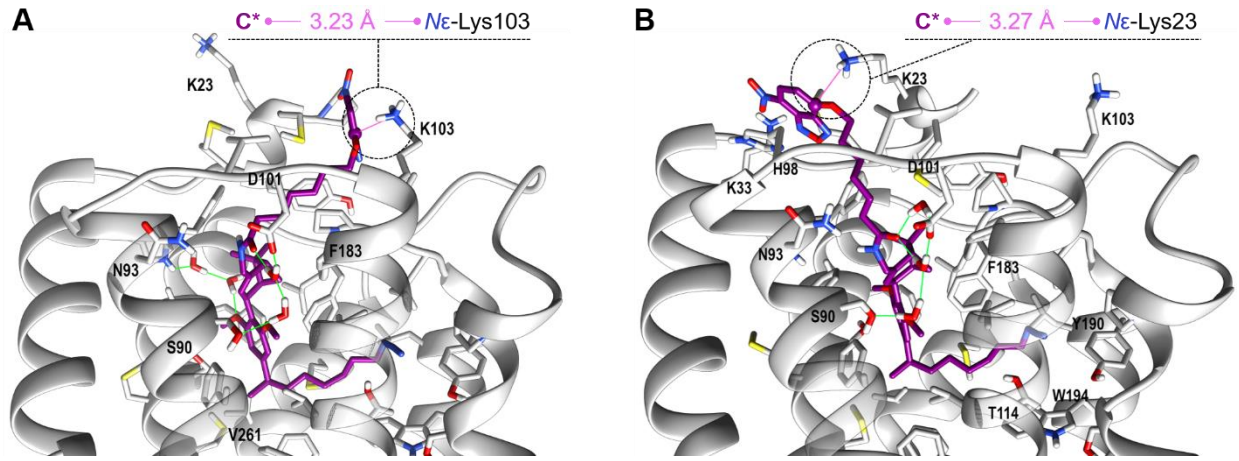


**Figure 2.** Representative frames from molecular dynamics simulation of **2b**-$CB_2R$ complex (PDB:5ZTY) featuring the shortest distance between the electrophilic *O*-NBD carbon (C*) of **2b** and $Lys103^{3.22}$ (**A**) and $Lys23^{NTER}$ (**B**) *N*ε atoms.

We used this structure in docking studies for the design of probes **2a-e** comprising **1a** and *O*-NBD. Prior work has highlighted the critical role of the linker type and length on the success as well as rate of target labeling.[47,63,67] This guided the selection of optimal linker length, which positions the electrophilic *O*-NBD carbon (C*) closest to the lysines. The hydrophobic lining of the exit channel from the orthosteric binding site suggested selection of alkyl linkers. Consequently, $CB_2R$ targeting appeared optimal with a heptanoyl linker (—HNOC$(CH_2)_6$—) featuring **2b**.[68]

To gain further insight into the conformational preferences and binding mode of **2b**, we conducted two independent 1 μs molecular dynamics (MD) simulations using Amber20 program. Both inactive (MD1, PDB:5ZTY)[69] and active (MD2, PDB:6PT0)[66] conformations of $CB_2R$ were used as starting points to enhance MD sampling and reduce potential biases from receptor conformation. The inactivating mutations present in PDB:5ZTY were back-mutated to wild-type residues before MD simulations. The same starting docking pose was used for both MD simulations since the conformation of the binding site is well-conserved in the two structures. The energy-minimized complexes were embedded in a pre-equilibrated palmitoyl-oleoyl-phosphatidyl-choline (POPC) lipid bilayer and solvated in an aqueous medium using the CHARMM-GUI web-interface.[70,71] Constant pressure and temperature (NPT) MD simulations were carried out at 310 K and 1 atm with the pmemd.cuda module of the Amber20 package,[72] using ff14SB (proteins), lipid 14 (lipids), and gaff (ligands) force field parametrizations (see SI for details).

Analysis of MD trajectories showed that **2b** adopts a canonical phytocannabinoid-like L-shaped conformation, forming van der Waals interactions with the hydrophobic residues lining the orthosteric site and engaging in π-π stacking with $Phe183^{ECL2}$. The amide group interacts with a network of water-mediated hydrogen bonds with $Asn93^{2.63}$, while the azide group, previously found critical to confer affinity and selectivity,[35] engages in polar interactions with $Thr114^{3.33}$ and $Tyr190^{5.39}$. The heptanoyl linker forms hydrophobic contacts with residues inside the helix bundle, while the *O*-NBD group docks on the extracellular rim of the helix bundle.

The rmsd analysis of MD1 and MD2 trajectories shows a similar trend in ligand fluctuations (see SI Figure S1). The fluctuations of **2b** and the ligand without linker (as the *N*-acetamide derivative of **1a**) were separately evaluated to uncouple the effect of the flexible linker from the rest of the molecule. Overall, the flexibility of the linker, mirrored by the increased fluctuation observed after its inclusion in the rmsd calculation, does not affect stability of the ligand within the orthosteric site. This suggests that the conjugate with NBD does not destabilize the ligand and that the linker provides adequate length to allow exiting the binding site without detrimental interactions between **2b** and $CB_2R$.

Subsequently, the propensity of the proximal lysine residues $Lys23^{NTER}$ and $Lys103^{3.22}$ to adopt spatial arrangements suitable for nucleophilic attack was evaluated by monitoring the distances between electrophilic carbon C* in **2b** and the lysine *N*ε atoms (see SI Figure S2). In MD2 simulation the distance between the electrophile and either of the two lysines was similar. In contrast, however, two main conformational basins were identified in MD1 simulation where a transition was observed from an initial shorter distance between electrophile and $Lys103^{3.22}$ (Figure 2A) to $Lys23^{NTER}$ (Figure 2B). The final conformation was stabilized by favorable interactions of the *O*-NBD group with $CB_2R$; π-π stacking of benzofurazan with $His98^{ECL1}$ and a polar interaction between the nitro group and $Lys33^{1.32}$. This stabilized arrangement remained constant when the simulation was extended by further 300 ns. Notably, also in MD2 trajectory $His98^{ECL1}$ remains close to the *O*-NBD group of **2b** for a large fraction of time (see SI Figure S3) while the stabilizing π-π stacking with benzofurazan is observed in two out of ten representative configurations arising from cluster analysis. In conclusion, although both $Lys23^{NTER}$ and $Lys103^{3.22}$ in principle satisfy the requirements for them to act as nucleophiles, the data suggest that $Lys23^{NTER}$ may react preferentially because for this pose the *O*-NBD group is locked in position by additional stabilizing interactions and polarized toward substitution.

## Synthesis & Radioligand Binding Assay

We devised an efficient, convergent synthesis where **1a** was functionalized in the last step with the linker-reporter motif (Scheme 2). As such, a set of *O*-NBD probes **2a-e** was synthesized with linkers varying in carbon chain length from 6 to 10. For experiments that function as negative controls, *N*-NBD derivative **5** was prepared. This probe is unable to transfer the NBD cargo and thus only labels $CB_2R$ in a reversible fashion.

Alkyl ω-hydroxy esters **3a**-**e** were allowed to react with F-NBD and the esters hydrolyzed under acidic conditions to reveal the carboxylic acid. Finally, HATU-mediated amide bond formation with **1a** afforded **2a**-**e**. Hence, *O*-NBD probes **2a**-**e** were obtained rapidly in three steps in a sufficient overall yield (28 – 38%). *N*-NBD control probe **5** was accessed in an analogous fashion starting from ester **4**.

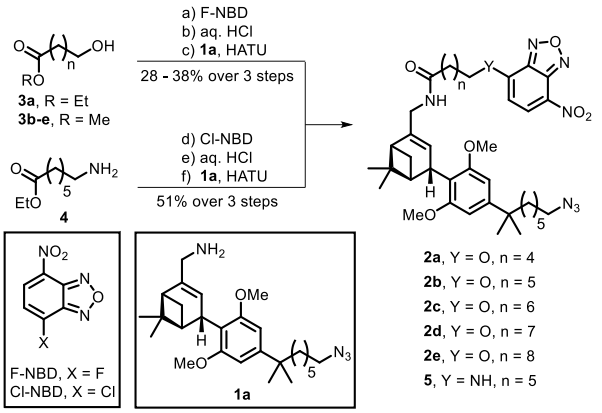


**Scheme 2.** Synthesis of *O*-NBD and *N*-NBD probes.[a]

[a]Reagents and conditions: (a) F-NBD, $Et_3N$, DMAP, $CH_2Cl_2$, rt, 40 – 61%; (b) aq. HCl, dioxane, 100 °C, 81 – 93%; (c) **1a**, HATU, *i*-$Pr_2NEt$, DMF, 0 °C – rt, 76 – 90%; (d) Cl-NBD, $NaHCO_3$, MeOH, rt, 92%; (e) aq. HCl, dioxane, 100 °C, 83%; (f) **1a**, HATU, *i*-$Pr_2NEt$, DMF, rt, 67%.

The *in vitro* pharmacological profile of *O*-NBD probes **2a**-**e** was evaluated in radioligand competition binding studies using [$^3$H]CP55,940 and membrane preparations of Chinese hamster ovary (CHO) cells expressing human $CB_1R$ ($hCB_1R$), $CB_2R$ ($hCB_2R$) or mouse $CB_2R$ ($mCB_2R$) (Table 1). All probes **2a**-**e** emerged as high affinity binders for $hCB_2R$ with $K_i$ values of 53 nM, 49 nM, 91 nM, 55 nM and 74 nM, respectively. Probes **2a**-**e** were avid binders of $mCB_2R$, albeit with decreased potency in comparison to the $hCB_2R$ ortholog. Probes **2b**, **2d** and **2e** also demonstrated excellent selectivity over the closely related $hCB_1R$ ($hK_i$ ratio $CB_1R/CB_2R$ > 100). These data validate the *in silico*-guided probe design, which yielded probes with excellent *in vitro* binding profiles.

**Table 1. Radioligand Competition Binding Assay With *O*-NBD LDC Probes.**[†]

| | | $K_i$ [nM] | | | |
|---|---|---|---|---|---|
| Cpd. | n | $hCB_1R$ | $hCB_2R$ | $mCB_2R$ | $hK_i$ ratio ($CB_1R/CB_2R$) |
| **2a** | 4 | 5207 | 53 | 198 | 98 |
| **2b** | 5 | 6039 | 49 | 443 | 123 |
| **2c** | 6 | 4130 | 91 | 377 | 45 |
| **2d** | 7 | >10000 | 55 | 641 | >182 |
| **2e** | 8 | >10000 | 74 | 351 | >135 |

[†][$^3$H]-CP55,940 was used to establish affinity ($K_i$) values in the radioligand binding assay with membrane preparations from CHO cells overexpressing $hCB_1R$, $hCB_2R$, or $mCB_2R$.

The pattern of molecular interactions observed during MD simulations provides insight for the observed trend involving stronger binding of **2a**-**e** toward $hCB_2R$ over the mouse ortholog. This could be ascribed to the human to mouse Val261$^{6.51}$Ala, Ser90$^{2.60}$Asn and Asn93$^{2.60}$Ile amino acid replacements. Val261$^{6.51}$ sidechain forms stabilizing hydrophobic interactions with the dimethyl group of the azidoheptyl substituent on the arene, which are absent in the mouse ortholog incorporating an alanine residue. Ser90$^{2.60}$Asn and Asn93$^{2.60}$Ile substitutions alter the steric hindrance of the ligand binding site and disrupt the network of water-mediated H-bonds, respectively. The drastic drop in affinity observed toward $CB_1R$ cannot be fully explained by the $CB_2R$ and $CB_1R$ amino acid residue substitutions alone. Thus, we speculate that significant contributions arise from the differences in ligand accessibility to the $CB_2R$ versus $CB_1R$ binding sites, as reported for the parent ligand of **1a**, HU-308.[73,74]

## TR-FRET-Based Assay to Assess Covalent NBD Transfer to $CB_2R$

The binding data for **2a**-**e** suggest that conjugation of **1a** with the electrophilic *O*-NBD motif is well tolerated. In previous work on ligand directed chemistry, covalent labeling was validated by Western blotting,[53] mass spectrometry,[46,75,76] UV-Vis spectroscopy[63] or time-resolved Förster resonance energy transfer (TR-FRET).[77] All of these approaches suffer from disadvantages. Western blotting along with mass spectrometry can be laborious and omit early time points, with the latter suggesting erroneous labeling rate for rapid reactions and resulting in inaccurate information of required incubation time. The use of UV-Vis spectroscopy can inform on the type of modified residue, however, its use is limited to reactions wherein covalent transfer leads to changes in spectral properties. The TR-FRET experiments as applied previously[77] do not give real-time insight into the rate of covalent labeling nor suggest the amino acid residue being modified.

To improve on the shortcomings of the reported methods, we aimed to exploit the spectral differences between *O*-NBD and *N*-NBD in combination with the temporal resolution offered by TR-FRET (Figure 3A).[78] As such, covalent labeling could be monitored in real time from the very start of the experiment following probe addition. As an added benefit, the intensity and wavelength of emission would inform on the type of residue involved in the covalent modification. In our TR-FRET binding assay, membrane preparations of human embryonic kidney cells (HEK293) overexpressing SNAP-tagged $CB_2R$ were labeled with a terbium-based FRET donor (SNAP-Lumi4-Tb). Upon irradiation ($\lambda$ = 337 nm), the Tb donor initiates energy transfer to a proximal acceptor and the measured acceptor to donor emission ratio provides direct insight into the covalent labeling. Since probes **2a**-**e** carry an alkyl *O*-NBD group and are hence non-fluorescent,[64,65] increase of emission at $\lambda_{em}$ = 520 nm indicates covalent *O*- to *N*- transfer of NBD.

Incubation of SNAP-$CB_2R$ membrane preparation with **2b** led to gradual increase of the FRET emission ratio (Figure 3B). Addition of a validated $CB_2R$ antagonist/inverse agonist, SR-144,528 ($hCB_2R$ $K_i$ = 13 nM),[79] following 120 min incubation did not lead to decrease in the signal intensity, corroborating successful NBD covalent transfer to a lysine residue. Investigation of the maximal specific TR-FRET ratio attained upon varied concentration and incubation time demonstrated that **2b** (100 nM) achieved complete covalent labeling within the 120 min incubation window (see SI Figure S4).

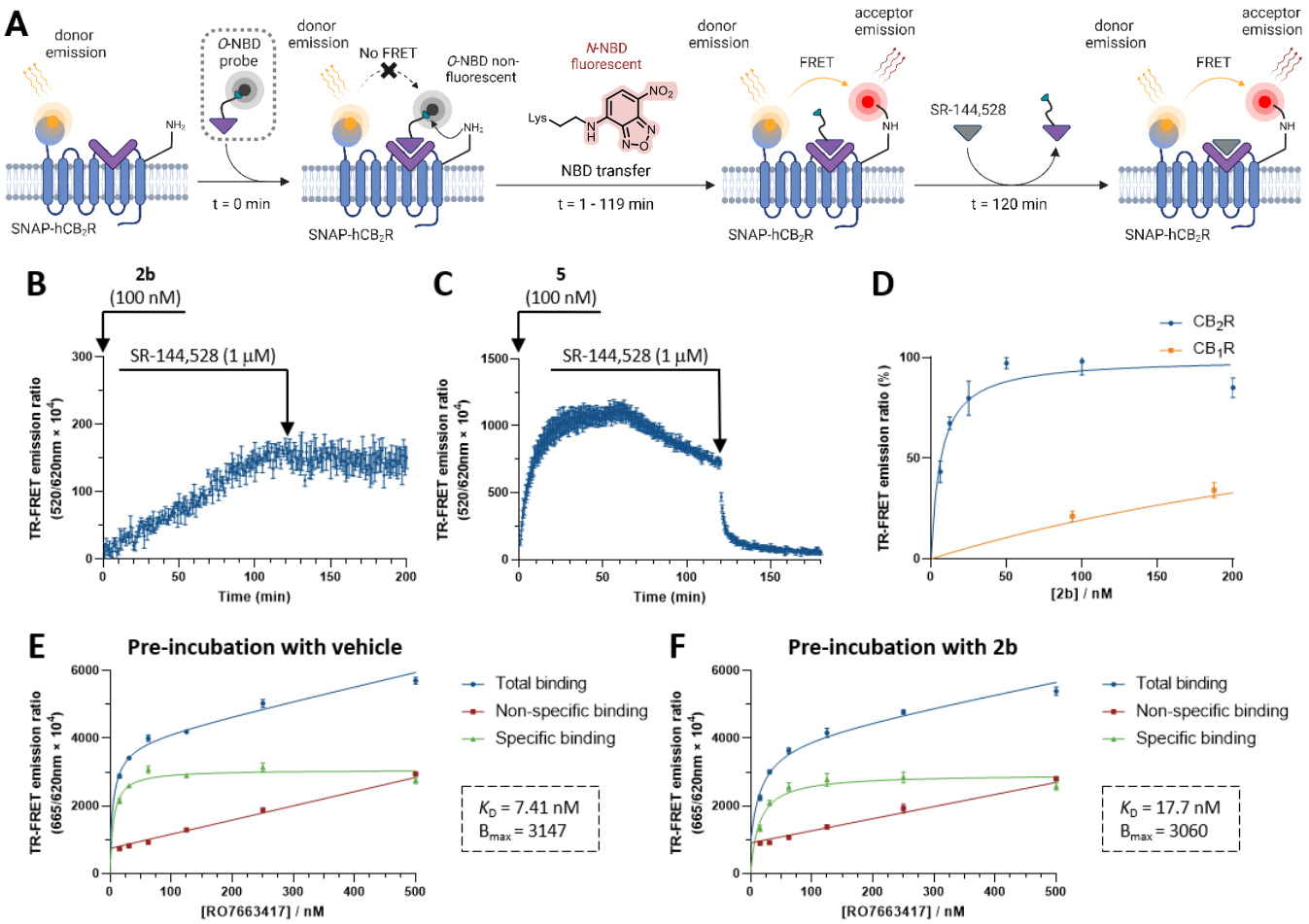


**Figure 3.** TR-FRET based characterisation of covalent NBD transfer to $CB_2R$; **A** Schematic flowchart of the TR-FRET experiment to investigate cargo transfer of *O*-NBD probes **2a-e**.[22] **B** SNAP-Lumi4-Tb labelled $CB_2R$ membranes were treated with *O*-NBD probe **2b** (100 nM). Following incubation for 120 min at 25 °C SR-144,528 (1 µM) was added. **C** SNAP Lumi-4-Tb labelled $CB_2R$ membranes were treated with *N*-NBD probe **5** (100 nM). Following incubation for 120 min at 25 °C SR-144,528 (1 µM) was added. **D** Saturation binding profile following a 2 h incubation at 37 °C with **2b** using a membrane preparation of HEK293 cells expressing either $CB_1R$ or $CB_2R$, previously labelled with SNAP-Lumi4-Tb. SNAP-Lumi4-Tb labelled $CB_2R$ membranes were treated with either vehicle (0.1% DMSO, **E**) or **2b** (100 nM, **F**) for 2 h at 37 °C prior to a saturation binding analysis of an Alexa647 functionalized $CB_2R$ selective probe, RO7663417.

Probes **2a** and **2c** achieved reduced signal intensity in comparison to **2b** (see SI Figure S5). As seen for **2b,** probes **2d** and **2e** also demonstrated good covalent labeling efficiency (see SI Figure S5). Hence, due to their excellent affinity and selectivity for $CB_2R$ in the radioligand study, combined with the strong signal in the TR-FRET assay, probes **2b**, **2d** and **2e** were the best suited candidates for future investigations. From this subset, the shorter, less lipophilic linker of **2b** in comparison to **2d** and **2e** was deemed superior as it was expected to confer improved target specificity and overall physicochemical properties, particularly lower lipophilicity.

As a control experiment, an analogous study was performed with probe **5**, which incorporates identical ligand and heptanoyl spacer as **2b**. However, it is incapable of undergoing transfer because it features an *N*-linked NBD fluorophore (Figure 3C). Incubation with **5** led to an increase in the FRET emission ratio (receptor binding), however, the addition of SR-144,528 dramatically decreased the signal intensity. This observation implies that probe **5** was displaced in a competitive fashion following SR-144,528 addition. These results collectively suggest that the ligand for the $CB_2R$ binding site can be displaced from the orthosteric site following NBD transfer by **2b**. The novel fluorogenic aspect applied in the TR-FRET assay enables rapid validation that a lysine residue proximal to the binding site of $CB_2R$ is amenable to covalent modification.

Upon further profiling, *O*-NBD probes were not susceptible to hydrolysis (pH = 1 – 8, see SI Table S1). We also set out to investigate whether the excellent selectivity of **2b** established by radioligand binding as shown in Table 1, would be reflected in the TR-FRET assay. Measurement of saturation binding following 2 h incubation at 37 °C with the respective $CB_1R$ or $CB_2R$ membrane preparations revealed a 50-fold selectivity bias of **2b** for $CB_2R$ over $CB_1R$, which is in agreement with the radioligand binding assay (Figure 3D).

Finally, we have investigated whether the covalent functionalization, proximal to the orthosteric site, affects capacity of $CB_2R$ to bind other ligands. To this end, $CB_2R$ membrane preparations were incubated with either vehicle (0.1% DMSO) or **2b** (100 nM). Readout of the TR-FRET ratio in the green channel at $\lambda_{em}$ = 520 (*N*-NBD signal) showed an intense response with **2b** incubated membranes compared to a background baseline signal of vehicle (see SI Figure S6). Subsequently, the

binding profile of a $CB_2R$ selective proprietary ligand RO7663417,[80] functionalized with an orthogonal fluorophore (Alexa647, $\lambda_{em}$ = 665 nm), was evaluated in a saturation binding assay in the red channel using the same membrane preparations. Remarkably, RO7663417 demonstrated essentially identical binding profile, $K_D$ and $B_{max}$ in membranes incubated with a vehicle (Figure 3E) or **2b** (Figure 3F). These results provide experimental evidence that the ability of orthosteric ligands to bind $CB_2R$ remains unaffected by the covalent modification proximal to the binding site.

## Universal Cargo Delivery Platform - *N*-Sulfonyl Pyridone & *N*-Acyl-*N*-Alkyl Sulfonamide

### Synthetic Design

The *O*-NBD probe **2b** demonstrated that covalent cargo transfer to a lysine residue of $CB_2R$ is feasible. However, owing to the intrinsic reactivity of **2b**, modification is exclusively restricted to covalent introduction of an NBD fluorophore. In this respect, the photophysical properties of the NBD fluorophore are suboptimal for cellular experiments due to its low quantum yield and tendency to photobleach.[81] Accordingly, we aimed to expand the repertoire of deliverable cargos, introduce a handle to tailor physicochemical properties, and design probes suitable for experiments in live cells.

In 2017 the Hamachi group reported ligand-directed sulfonylation of tyrosine and lysine residues facilitated by *N*-sulfonyl pyridones (*N*-SP).[52] Despite the attractiveness of the system, to the best of our knowledge, this is the only report utilizing LDC *N*-SP probes. We suspect that a significant hurdle to broader adoption of the *N*-SP chemistry is the currently available synthetic route. It suffers from a number of limitations, including linearity, production of undesired *O*-pyridone constitutional isomers, and poor yields overall.

*N*-Acyl-*N*-alkyl sulfonamide (NASA) constitutes a complementary electrophile for covalent linking. It is selective for ligand-directed acylation of lysine residues and has lately been the electrophile of choice due to its rapid labeling kinetics ($k_2 = 10^4\ M^{-1}\ s^{-1}$).[53] The application of NASA electrophiles includes generation of small-molecule LDC probes,[53,82] LDC aptamers,[83] development of ligand screening assays,[84] modification of protein-protein interactions[85] and targeted protein degradation.[86] In many of the reported cases, the synthesis of the LDC probes commenced from precious starting materials which are subjected to laborious synthesis sequences. Consequently, the resulting applications may be restricted to conveniently available ligands and fluorophores.

In a single instance, Hamachi reported amide bond formation in presence of the *N*-SP electrophile followed by a copper-catalyzed azide-alkyne cycloaddition (CuAAC) to assemble the LDC probe albeit in 2% yield over the two steps.[52] We thus hypothesized that further investigations could yield methods to assemble LDC probes incorporating either *N*-SP or NASA electrophiles by robust orthogonal functionalization in the final steps with cargo and ligand. Hence, we envisioned a streamlined assembly route for probes involving central *N*-SP and NASA platform reagents (Scheme 3A). This strategy significantly expands the available targets that can be engaged as well as the range of deliverable cargos by allowing a wide range of ligands and fluorophores to be efficiently incorporated into the LDC probes. The availability of fluorophores bearing azides and ligands incorporating amines suggested the use of CuAAC and amide bond formation, respectively.

Synthesis of LDC probes commenced with ω-amino alkyl esters **6a-c** (Scheme 3B). *En route* toward *N*-SP platforms, the esters were allowed to react with 6-hydroxynicotinic acid to yield 6-hydroxynicotinamides **7a-c**. The reported conditions for the formation of *N*-SP using $Et_3N$ in DMF yielded a 3:1 mixture favoring the undesired *O*-SP over the *N*-SP constitutional isomer, consistent with the low yields reported by Hamachi.[52] Further investigations by us led to conditions in which the *N*-SP constitutional isomer is formed preferentially using *t*-BuOK in THF at –78 °C (*O*-SP : *N*-SP = 1:10) in good yield (68 – 72%) to give platform reagents **9a-c**.

Complementary NASA platform reagent **13** was accessed rapidly in three steps by reacting **6b** with 4-sulfamoylbenzoic acid to yield **12**, followed by *N*-acylation with 4-pentynoic acid and finally *N*-alkylation with iodoacetonitrile. Platform reagents **9a-c** and **13** were functionalized with fluorophores by CuAAC to yield **10a-d** and **14**, respectively. During the final amide bond formation with the targeting ligand *N*-SP and NASA electrophilic motifs are highly susceptible to degradation, therefore efficient activation of the carboxylic acid, produced following ester deprotection in **10a-d** and **14**, was required for a rapid and selective reactivity with amines.

Unfortunately, many methods for the activation of carboxylic acids are either too harsh or involve nucleophiles (e.g. DMAP, HOBt) that can facilitate degradation of the *N*-SP and NASA motifs. We noted that the amide bond can be formed selectively in presence of the highly electrophilic *N*-SP and NASA motifs by employing HATU in a TFA/*i*-$Pr_2NEt$ mixture that serves to buffer out the nucleophilic HOAt. This discovery allowed us to complete the modular synthesis and link the $CB_2R$ homing ligands **1a-b** to yield the respective *N*-SP (**11a-e**) and NASA (**15**) probes.

### TR-FRET-Based Assay to Evaluate Covalent Transfer of *N*-SP & NASA LDC Probes

We have subsequently tested efficiency of probes **11a-e** and **15** toward transfer of their cargo by means of TR-FRET. Each probe was tested with analogous experiments previously described for **2b** (Figure 3A): incubation of $CB_2R$ membrane preparation with probe, followed by addition of SR-144,528 to dissociate unreacted probe (see Figure 4 and SI Figures S7-S9). We evaluated the efficiency of covalent modification as the ratio of FRET intensity prior to addition of SR-144,528 to the FRET intensity post addition at the end of measurement.

Variation in the spacer length separating the ligand and *N*-SP electrophile yielded probes with pentanoyl (**11a**), heptanoyl (**11b**) and nonanoyl (**11c**) exit vectors. Upon incubation with the membrane preparation for 120 min at 25 °C, the probes demonstrated efficiency of covalent labeling of 11.3% ± 2.7%, 13.6% ± 1.9% and 9.8% ± 3.4%, respectively. Probe **11d** was prepared from ligand **1b** where the terminal azide, which was previously shown to increase affinity for $CB_2R$ by up to 15-fold,[35] was deleted.

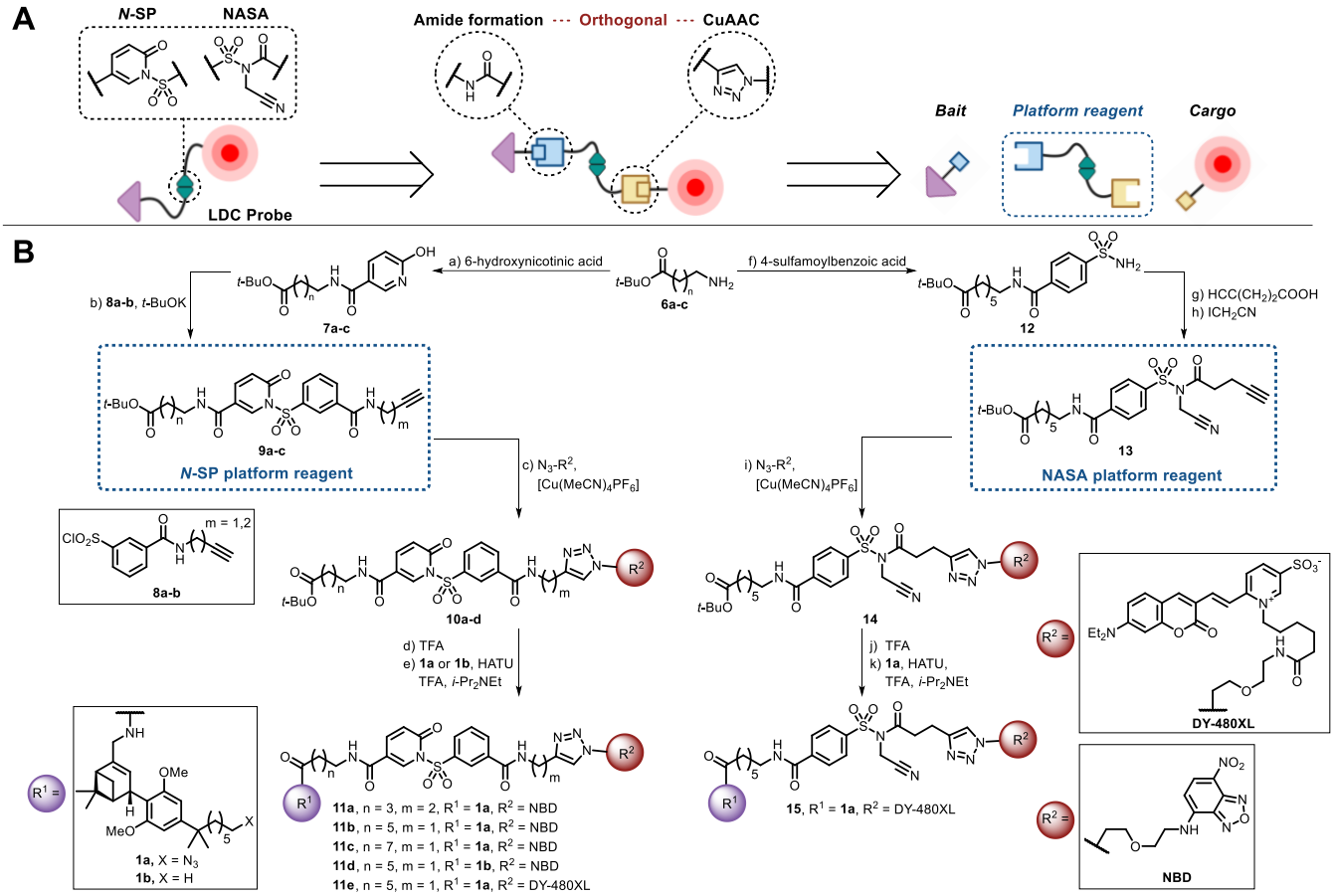


**Scheme 3. A** Proposed disconnection of *N*-SP and NASA LDC probes to their respective platform reagents.[22] **B** Synthesis of *N*-SP and NASA probes.[a] [a]Reagents and conditions: (a) 6-hydroxynicotinic acid, EDCI·HCl, $Et_3N$, DMF, rt, 67 – 87%; (b) **8a** or **8b**, *t*-BuOK, THF, –78 °C to rt, 68 – 72%; (c) **$N_3$-DY-480XL** or **$N_3$-NBD**, $[Cu(MeCN)_4]PF_6$, AcOH, $CH_2Cl_2$, rt, 73 – 88%; (d) TFA, $CH_2Cl_2$, rt; (e) **1a** or **1b**, HATU, TFA, *i*-$Pr_2NEt$, DMF, 0 °C to rt, 72 – 92% over two steps; (f) 4-sulfamoylbenzoic acid, EDCI·HCl, HOBt·$H_2O$, *i*-$Pr_2NEt$, DMF, rt, 67%; (g) 4-pentynoic acid, EDCI·HCl, DMAP, *i*-$Pr_2NEt$, DMF, rt, 70%; (h) $ICH_2CN$, *i*-$Pr_2NEt$, DMF, rt, 78%; (i) **$N_3$-DY-480XL**, $[Cu(MeCN)_4]PF_6$, AcOH, $CH_2Cl_2$, rt, 94%; (j) TFA, $CH_2Cl_2$, rt; (k) **1a** , HATU, TFA, *i*-$Pr_2NEt$, DMF, 0 °C to rt, 66% over two steps.

Accordingly, **11d** demonstrated reduced covalent transfer (3.8% ± 6.4%) within the 120 min incubation time and corroborated the affinity-driven nature of our labeling approach. *N*-SP probe **11e** bearing a red-emitting DY-480XL dye with large Stokes shift (see SI Figure S10) suitable for *in vivo* imaging demonstrated decent covalent transfer in 120 min (25.2% ± 1.4%).

When the incubation time of probes **11a-e** was extended to 20 h the labeling yields improved significantly (**11a** = 46.9% ± 3.2%, **11b** = 49.6% ± 1.8%, **11c** = 59.6% ± 3.8%, **11d** = 37.5% ± 2.7%). Notably, following 20 h incubation time, **11e** demonstrated complete covalent transfer of its fluorophore, as indicated by our FRET assay (105.7% ± 7.2%). When the experiment was performed at a physiologically relevant temperature (37 °C) the rate was enhanced and **11e** showed 53.5% ± 9.6% cargo transfer after 120 min. By measuring saturation binding we were pleased to see that **11e** demonstrated a 119-fold selectivity for $CB_2R$ over $CB_1R$ in our TR-FRET assay (see SI Figure S11).

Finally, switching the *N*-SP electrophile of **11e** to the more reactive NASA motif yielded probe **15**. Accordingly, the modification greatly improved the rate of covalent labeling and **15** achieved complete transfer (100.8% ± 4.1%) within the 120 min incubation time at 37 °C.

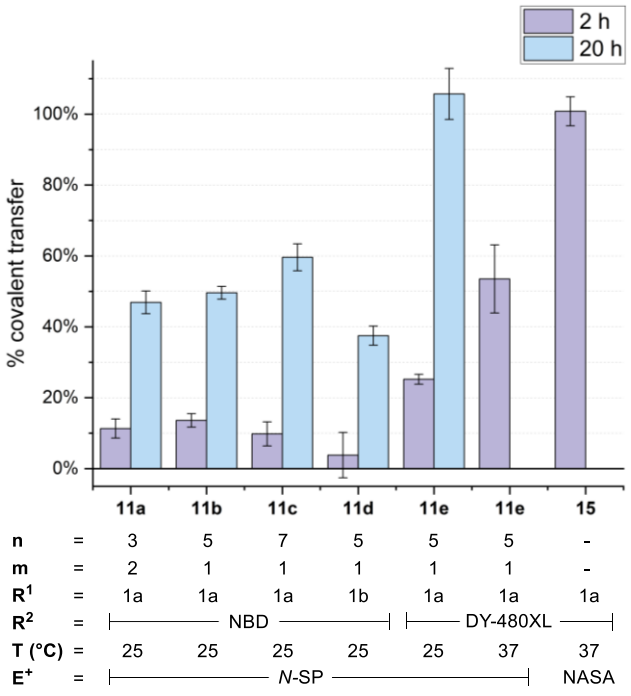

**Figure 4.** TR-FRET based evaluation of covalent cargo transfer of probes **11a-e** (100 nM) and **15** (200 nM) following a 2 h or 20 h incubation at 25 °C or 37 °C. The percentage shown for each probe represents a quotient of its TR-FRET ratio determined prior to addition of SR-144,528 and at the end of measurement post addition. Mean ± SEM, $N = 3$.

## Molecular Dynamics Simulation of Probe 15

Subsequently, the best performing probe **15** was investigated by MD simulations. The conformational space accessible to the NASA linker of **15** and its molecular interactions within the ligand binding site were explored with two independent 1 μs MD simulations to identify residues that could serve as nucleophiles. The simulations were run with the same computational protocol adopted for **2b**, using a truncated form of **15** in which the fluorophore was deleted, implied stable binding of the probe in the orthosteric site (see SI Figure S12). The MD1 and MD2 simulations were in agreement in finding that both $Lys23^{NTER}$ and $Lys103^{3.22}$ are at suitable distances for acylation (see SI Figures S13–S15). Furthermore, due to greater linker length and flexibility, the NASA electrophile is also in proximity to $Lys33^{1.32}$ (see SI Figures S16–S17). In the simulations, $His98^{ECL1}$ stabilized the linker by forming either direct or water-mediated hydrogen bonds with the NASA group. Moreover, $His98^{ECL1}$ remained spatially close to the NASA electrophile over a considerable fraction of the simulated period suggesting it could assist in the covalent modification of $CB_2R$ by **15** (see SI Figure S17).

## Application of $CB_2R$ LDC Probes in Live Cells

### Conventional Flow Cytometry

Having established the success of covalent cargo transfer of the probes and target specificity *in vitro*, we next turned our attention to investigate labeling of $CB_2R$ in live cells. The best performing probes of each electrophile type, namely *O*-NBD (**2b**), *N*-SP (**11e**) and NASA (**15**), were studied by means of conventional flow cytometry (FC).

To this end, HEK293 T-REx cells expressing $hCB_2R$ along with HEK293 wild-type cells, which do not express $CB_2R$,[87,88] were incubated with an LDC probe at concentrations that ranged from 6.25 nM – 200 nM and subsequently analyzed by means of FC. The FC data of probes **2b**, **11e** and **15** implied significantly increased fluorescence intensity in cells expressing $hCB_2R$ (Figure 5A, SI Figures S18A and S19A) in comparison to wild-type cells (Figure 5B, SI Figures S18B and S19B). Furthermore, the fluorescence signal of all three probes was substantially reduced upon pre-incubation with SR-144,528 implying excellent $CB_2R$ binding specificity in a cellular setting. *O*-NBD probe **2b** demonstrated clear specific binding signal in $CB_2R$ expressing cells when compared to wild-type. However, the signal was relatively weak and fairly high levels of non-specific binding were detected upon pre-incubation with SR-144,528. *N*-SP and NASA probes **11e** and **15** displayed excellent specific binding in $CB_2R$ expressing cells with minimal background signal in cells pre-incubated with SR-144,528. For both **11e** and **15** the fluorescent signal was substantially more intense in comparison to **2b** and their target engagement was highly specific in $CB_2R$ expressing cells with virtually no binding in the wild-type cells. The excellent specificity of the new probes in FC experiments corroborates our earlier results of in-gel fluorescence and CEREP off-target screen with close derivatives of **11e** and **15,** which feature the same ligand[89] and even ligand-fluorophore,[30] that yielded a highly $CB_2R$-specific binding profile.

### Imaging Flow Cytometry

The conventional FC investigation allowed rapid quantitative assessment of total cell fluorescence, while complementary imaging flow cytometry (IFC)[90] experiments additionally yield quantitative information about localization of a fluorophore across 10,000 cells. In addition to validating binding specificity IFC experiments allowed us to distinguish $CB_2R$ visualized intracellularly in comparison to receptors restricted to the plasma membrane. Live HEK293 T-REx cells expressing $hCB_2R$ were incubated with either **2b**, **11e** or **15** (see SI Figures S20–S23). The results were compared to cells pre-incubated with SR-144,528 before addition of the LDC probe. The average of the 10,000 generated cellular images was interrogated to yield an overall representation of binding specificity and localization of labeling.

In agreement with results from the conventional FC experiments, all three probes **2b**, **11e** and **15** demonstrated labeling in $hCB_2R$ expressing cells (Figure 5CDE, SI Figures S20AB, S21ABC and S22ABC) which was substantially reduced in cells pre-incubated with SR-144,528 (Figure 5FGH, SI Figures S20CD, S21DEF and S22DEF). The fluorescence intensity for **2b** was 1.9-fold greater in comparison to control and was reduced by 16% in cells pre-incubated with SR-144,528 as determined by median fluorescence intensity (MFI) (see SI Figure S24 and Table S2). Compared to control, DY-480XL functionalized probes **11e** and **15** showed 9.4-fold and 8.5-fold increase in fluorescence intensity, respectively (see SI Figures S25-S26 and Table S3). The fluorescence signal of **11e** and **15** was reduced in cells pre-incubated with SR-144,528 by 38% and 52%, respectively, as determined by MFI.[91]

Subsequently, we analyzed individual images of the whole gated cell population to discern populations of internalized and membrane bound $CB_2R$. Median internalization quotient (MIQ) was used to compare internal to whole cell fluorescence, where a smaller number indicates less $CB_2R$ internalization (see SI for details). Incubation with **2b** visualized $CB_2R$ localized at the membrane and intracellularly to a similar extent with MIQ = 0.91. Compared to **2b**, cells exposed to **11e** or **15** demonstrated receptor internalization to a smaller degree and visualized $CB_2R$ primarily confined to the plasma membrane with MIQ = 0.46 and MIQ = 0.68, respectively. Collectively, the data showcase the high affinity and excellent specificity of LDC probes **2b**, **11e** and **15** for $CB_2R$ in living cells. Moreover, the DY-480XL functionalized **11e** and **15** displayed intense fluorescent signal and allowed bright visualization of $CB_2R$, attesting to their suitability for application in cellular settings.

## Fluorescence Microscopy in $CB_2R$ Expressing Cells

Due to the relatively high lipophilicity of $CB_2R$ ligands, we wanted to verify in an independent experiment that our probes were labeling $CB_2R$, as opposed to accumulating non-specifically within the cellular membranes. We therefore used lentiviral transduction to produce a cell line stably expressing $hCB_2R$ *N*-terminally fused to a SNAP-tag [AtT-20(SNAP-$hCB_2R$)]. Live AtT-20(SNAP-$hCB_2R$) cells were co-incubated with **15** (2 μM), SNAP-Surface-649 (100 nM) to fluorescently label the SNAP-tags, and Hoechst-33342 (100 nM) to label the nuclei, for 45 min; then the cells were imaged by confocal fluorescence microscopy (see Figure 6ABC and SI Figure S27).

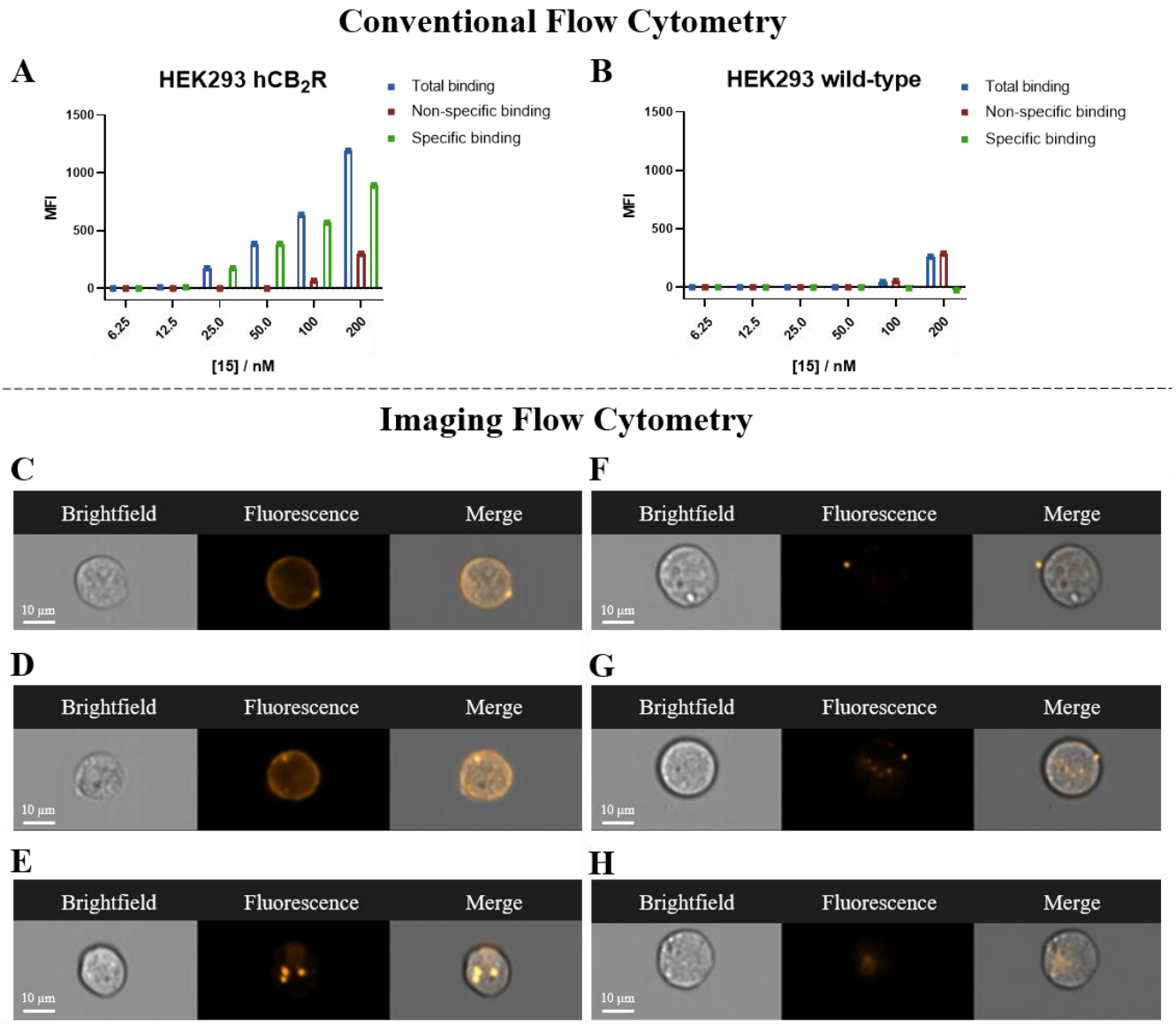


**Figure 5.** Conventional and imaging flow cytometry studies with LDC probe **15**; Conventional flow cytometry of HEK293 T-REx hCB$_2$R (**A**) and HEK293 wild-type cells (**B**) upon incubation with **15** (6.25 – 200 nM). The mean fluorescence intensity (MFI) is shown with subtracted background. Non-specific binding was determined with SR-144,528 (10 µM). Representative frames from imaging flow cytometry experiments using HEK293 T-Rex hCB$_2$R and **15** (210 nM) with CB$_2$R visualized primarily at the plasma membrane (**C**, MIQ < –1), at both membrane and intracellularly (**D**, MIQ = –0.5 – 0.5), and intracellularly (**E**, MIQ > 2). The same experiment with cells pre-incubated with SR-144,528 (10 µM) showing fluorescence restricted to the plasma membrane (**F**, MIQ < –1), at both membrane and intracellularly (**G**, MIQ = –0.5 – 0.5), and intracellularly (**H**, MIQ > 2). Median internalization quotient (MIQ) compares internal to whole cell fluorescence, where smaller number corresponds to less CB$_2$R internalization. For additional exemplary frames, histograms and analysis see SI.

We observed a strong DY-480XL signal on the plasma membrane of the cells, as well as puncta intracellularly, which could represent internalized receptors (Figure 6A, left). This signal co-localized with the far-red SNAP-dye signal (Figure 6A, right), confirming that **15** was successfully labeling the SNAP-tagged CB$_2$Rs.

Applying the same treatment to wild-type AtT-20 cells, which do not express CB$_2$Rs or SNAP-tags, resulted in a lack of DY-480XL or SNAP-Surface-649 at the plasma membrane, confirming that the dyes are labeling surface-expressed SNAP-hCB$_2$R (Figure 6B). To verify that **15** was labeling CB$_2$R by binding its orthosteric site, AtT-20(SNAP-hCB$_2$R) cells were pre-treated with SR-144,528 (20 µM), followed by **15**, SNAP-Surface-649, and Hoechst-33342 as before. Pre-treatment with SR-144,528 abolished the DY-480XL signal on the plasma membrane, while the SNAP-tags were still observed on the plasma membrane (Figure 6C). Combined, these results confirm that in living cells **15** specifically engages the orthosteric site of CB$_2$R prior to delivery of its cargo at the binding site periphery.

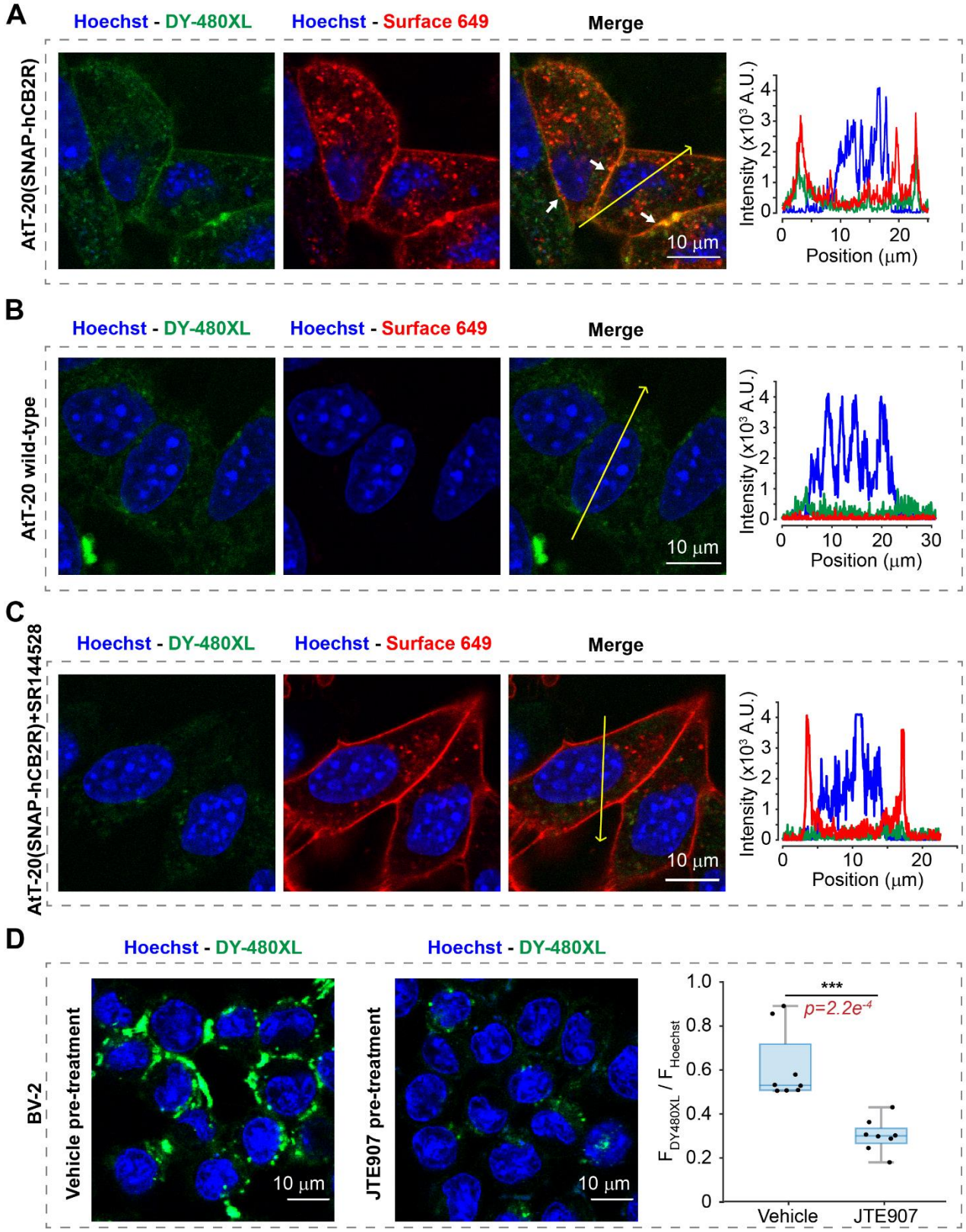


**Figure 6.** Fluorescence confocal microscopy with LDC probe **15**; Fluorescent labeling of $CB_2R$ using **15** (2 μM) to deliver DY-480XL by LDC chemistry in (**A**) AtT-20(SNAP-h$CB_2R$) cells, (**B**) AtT-20-wild-type cells, and (**C**) AtT-20(SNAP-h$CB_2R$) cells that were pre-treated with SR-144,528 (20 μM). Nuclei were stained with Hoechst33342 and white arrows highlight $CB_2R$ and SNAP-dye plasma membrane colocalization. Right panels indicate the intensity profile across the yellow line for Hoechst33342, DY-480XL, and SNAP-Surface-649 fluorescence. (**D**) Live BV-2 microglial cells were pre-treated with either vehicle (left) or $CB_2R$ antagonist JTE-907 (20 μM, center), then incubated with **15** (500 nM) and Hoechst33342 (1 μM) for 15 min and imaged by confocal microscopy. On the right is a boxplot showing normalized DY480-XL fluorescence of probe **15** in BV-2 cells pre-treated with a vehicle and JTE-907, respectively. The summarized data in the boxplot are an average over 8 images from 4 biological replicates, for each condition. Significance examined by a Student's two-sample t-test. ***$p < 0.001$

The promising performance of **15** in AtT-20 $CB_2R$ overexpressing cells compelled us to apply the probe in an endogenously expressing cell line. BV-2 cells are a murine-derived microglial cell line that has been applied extensively to study neuroinflammation,[92] neurodegeneration and, in particular, Alzheimer's disease.[93,94] Since BV-2 cells endogenously express $CB_2R$ and respond to cannabinoid ligands they were ideally suited for our study.[95,96]

To this end, live BV-2 cells were pre-treated with either vehicle (0.1% DMSO) or $CB_2R$ antagonist JTE-907[97] (20 μM) prior to addition of probe **15** (500 nM) and Hoechst33342 (1 uM) to visualize $CB_2R$ and nuclei, respectively. Subsequently, the BV-2 cells were investigated by live-cell confocal fluorescence imaging. Upon pre-treatment with a vehicle, intense DY480-XL fluorescence was observed stemming from the cytoplasm along with a strong signal delineating the perimeter of the BV-2 cells (Figure 6D, left). Pre-incubation with a $CB_2R$ antagonist JTE-907 significantly reduced intensity of the DY480-XL signal in comparison to vehicle (Figure 6D, center and right). These results confirm that **15** is capable to specifically visualize $CB_2R$ at endogenous expression levels.

## CONCLUSION

We reported herein novel synthetic access to a set of LDC probes incorporating *O*-NBD, *N*-sulfonyl pyridone (*N*-SP) and *N*-acyl-*N*-alkyl sulfonamide (NASA) electrophiles, which allowed covalent labeling of $CB_2R$ *in vitro*, in HEK293($hCB_2R$) T-Rex, AtT-20(SNAP-$hCB_2R$), and BV-2 microglial cell lines. With the aid of computational docking and molecular dynamics simulations, nucleophilic lysine residues suitable for affinity-driven covalent modification were identified peripheral to $CB_2R$ ligand binding site. The *in silico* inspired design of *O*-NBD probes **2a**-**e** yielded potent and selective $CB_2R$ binders, as evaluated by a radioligand binding assay. Further profiling of **2a**-**e** by a fluorogenic TR-FRET assay allowed rapid confirmation of their potential to transfer NBD in a covalent fashion to a lysine residue of $CB_2R$. Experimental evidence implied that the ability of other ligands to bind $CB_2R$ remained unaffected by the covalent cargo transfer proximal to the orthosteric site. The *N*-SP and NASA electrophiles were incorporated into the probe design to enable delivery of fluorophores suitable for cellular experiments. New convergent synthetic strategies were developed and successfully implemented to achieve *N*-SP and NASA probes **11e** and **15**, which bear a non-commercial $CB_2R$ targeting ligand **1a** and a red-emitting fluorophore, DY-480XL. As judged by the *in vitro* TR-FRET assay, both probes achieve complete covalent labeling of $CB_2R$, with probe **15** demonstrating superior rate of covalent modification. The best performing probes of each electrophile class, **2b**, **11e**, **15**, were tested in live cells by conventional and imaging flow cytometry experiments. DY-480XL functionalized probes **11e** and **15** demonstrated excellent specificity of binding to $CB_2R$ as implied by comparison of $CB_2R$ expressing HEK293 T-REx cells to wild-type cells across a range of concentrations. Imaging flow cytometry experiments with **11e** and **15** demonstrated clear visualization of plasma membrane bound $CB_2R$, which could be effectively blocked by pre-treatment with a $CB_2R$-selective competitive ligand, SR-144,528. Furthermore, target specificity was corroborated by colocalization studies performed with **15** in AtT-20(SNAP-$hCB_2R$) cells. Binding of **15** to the orthosteric site of $CB_2R$ prior to cargo delivery at the receptor's periphery was validated in AtT-20(SNAP-$hCB_2R$) cells by pre-incubation with SR-144,528 and supported the ligand-driven nature of covalent labeling. Finally, the significant value of **15** was highlighted by visualizing $CB_2R$ expressed at endogenous levels in the BV-2 microglial cell line.

It is important to note that the choice of a suitable electrophile is guided by the target protein and availability of nucleophilic amino acid residues proximal to the binding site. The *N*-SP and NASA preference for tyrosine and lysine residues, respectively, makes the LDC platform disclosed herein a complementary toolbox to investigate a vast space of protein targets by covalent modifications. Consequently, the convergent synthetic blueprint effectively expands the possibilities of covalent modification with respect to both deliverable cargoes and proteome targetable with non-commercial ligands. The need for reliable tools to study $CB_2R$ is emphasized by the growing evidence of the receptor's crucial role in a plethora of neuroinflammatory diseases. For example, the lifetime, trafficking and recycling of $CB_2R$, which are poorly understood, may be studied and elucidated with LDC probes.

We have reported the first probes to facilitate investigation of $CB_2R$ by LDC chemistry using our agonist ligand **1a**.[35] The study of a cellular setting with minimal perturbation (no agonist induced receptor internalization) would demand an antagonist ligand. Unfortunately, to date no antagonist ligand with sufficient selectivity and specificity for $CB_2R$ has been reported.[98] Once discovered, our novel synthetic platform promises to allow streamlined installation of a suitable $CB_2R$ targeting antagonist ligand to **14**. The fluorescent probes, chemistry and analytical methods described herein will find valuable application both in the research of $CB_2R$ and in the study of other protein targets by translation.

## ASSOCIATED CONTENT

**Supporting Information**. The Supporting Information is available free of charge on the ACS Publications website.

Experimental procedures and characterization data for all compounds.

## AUTHOR INFORMATION

### Corresponding Authors

*E-mail: erickm.carreira@org.chem.ethz.ch
*E-mail: dmitry.veprintsev@nottingham.ac.uk
*E-mail: frankja@ohsu.edu
*E-mail: uwe.grether@roche.com

### Notes

The authors declare the following competing financial interest: M.K., R.C.S., R.L.G., W.G., U.G. and E.M.C have filed a patent on $CB_2R$ selective LDC probes.

## ACKNOWLEDGEMENTS

We thank Ken Mackie for helpful discussions and providing BV-2 and AtT-20 cell lines. We are grateful to Björn Wagner for generating ASTA data and Isabelle Kaufmann for help with logistics. We thank René Arnold, Rainer Frankenstein and Stephan Burkhardt for their help with NMR measurements and the MoBiAS team for MS analysis. M.K. and R.C.S. gratefully acknowledge a fellowship by the Scholarship Fund of the Swiss Chemical Industry (SSCI). MD studies have been funded by project code PIR01_00011 "IBISCo", PON 2014-2020, for all three entities (INFN, UNINA and CNR). The ID7000C spectral cell analyzer was funded by the Biotechnology and Biological Sciences Research Council (BB/T017619/1). The ImageStreamX MKII imaging flow cytometer was funded by the Wellcome Trust (212908/Z/18/Z).

## REFERENCES

1. Munro, S.; Thomas, K. L.; Abu-Shaar, M. Molecular characterization of a peripheral receptor for cannabinoids. *Nature* **1993**, *365*, 61-65

2. Maccarrone, M. *New Tools to Interrogate Endocannabinoid Signalling: From Natural Compounds to Synthetic Drugs*; The Royal Society of Chemistry, 2021.

3. Galiegue, S.; Mary, S.; Marchand, J.; Dussossoy, D.; Carriere, D.; Carayon, P.; Bouaboula, M.; Shire, D.; Le Fur, G.; Casellas, P. Expression of

central and peripheral cannabinoid receptors in human immune tissues and leukocyte subpopulations. *Eur. J. Biochem.* **1995**, *232*, 54-61
4. Svizenska, I.; Dubovy, P.; Sulcova, A. Cannabinoid receptors 1 and 2 (CB1 and CB2), their distribution, ligands and functional involvement in nervous system structures – a short review. *Pharmacol., Biochem. Behav.* **2008**, *90*, 501-511
5. Turcotte, C.; Blanchet, M. R.; Laviolette, M.; Flamand, N. The CB2 receptor and its role as a regulator of inflammation. *Cell. Mol. Life Sci.* **2016**, *73*, 4449-4470
6. Guindon, J.; Hohmann, A. G. Cannabinoid CB2 receptors: a therapeutic target for the treatment of inflammatory and neuropathic pain. *Br. J. Pharmacol.* **2008**, *153*, 319-334
7. Pacher, P.; Mechoulam, R. Is lipid signaling through cannabinoid 2 receptors part of a protective system? *Prog. Lipid Res.* **2011**, *50*, 193-211
8. Dhopeshwarkar, A.; Mackie, K. CB2 Cannabinoid receptors as a therapeutic target-what does the future hold? *Mol. Pharmacol.* **2014**, *86*, 430-437
9. Pacher, P.; Kunos, G. Modulating the endocannabinoid system in human health and disease-successes and failures. *FEBS J.* **2013**, *280*, 1918-1943
10. Schatz, A. R.; Lee, M.; Condie, R. B.; Pulaski, J. T.; Kaminski, N. E. Cannabinoid Receptors CB1 and CB2: a characterization of expression and adenylate cyclase modulation within the immune system. *Toxicol. Appl. Pharmacol.* **1997**, *142*, 278-287
11. Griffin, G.; Fernando, S. R.; Ross, R. A.; McKay, N. G.; Ashford, M. L.; Shire, D.; Huffman, J. W.; Yu, S.; Lainton, J. A.; Pertwee, R. G. Evidence for the presence of CB2-like cannabinoid receptors on peripheral nerve terminals. *Eur. J. Pharmacol.* **1997**, *339*, 53-61
12. Viscomi, M. T.; Oddi, S.; Latini, L.; Pasquariello, N.; Florenzano, F.; Bernardi, G.; Molinari, M.; Maccarrone, M. Selective CB2 receptor agonism protects central neurons from remote axotomy-induced apoptosis through the PI3K/Akt pathway. *J. Neurosci. Res.* **2009**, *29*, 4564-4570
13. Stempel, A. V.; Stumpf, A.; Zhang, H. Y.; Ozdogan, T.; Pannasch, U.; Theis, A. K.; Otte, D. M.; Wojtalla, A.; Racz, I.; Ponomarenko, A.; Xi, Z. X.; Zimmer, A.; Schmitz, D. Cannabinoid Type 2 Receptors Mediate a Cell Type-Specific Plasticity in the Hippocampus. *Neuron* **2016**, *90*, 795-809
14. Li, Y.; Kim, J. Neuronal expression of CB2 cannabinoid receptor mRNAs in the mouse hippocampus. *Neuroscience* **2015**, *311*, 253-267
15. Lanciego, J. L.; Barroso-Chinea, P.; Rico, A. J.; Conte-Perales, L.; Callen, L.; Roda, E.; Gomez-Bautista, V.; Lopez, I. P.; Lluis, C.; Labandeira-Garcia, J. L.; Franco, R. Expression of the mRNA coding the cannabinoid receptor 2 in the pallidal complex of Macaca fascicularis. *J. Psychopharmacol.* **2011**, *25*, 97-104
16. Garcia-Gutierrez, M. S.; Garcia-Bueno, B.; Zoppi, S.; Leza, J. C.; Manzanares, J. Chronic blockade of cannabinoid CB2 receptors induces anxiolytic-like actions associated with alterations in GABA(A) receptors. *Br. J. Pharmacol.* **2012**, *165*, 951-964
17. Cabral, G. A.; Raborn, E. S.; Griffin, L.; Dennis, J.; Marciano-Cabral, F. CB2 receptors in the brain: role in central immune function. *Br. J. Pharmacol.* **2008**, *153*, 240-251
18. Stella, N. Cannabinoid and cannabinoid-like receptors in microglia, astrocytes, and astrocytomas. *Glia* **2010**, *58*, 1017-1030
19. Cabral, G. A.; Marciano-Cabral, F. Cannabinoid receptors in microglia of the central nervous system: immune functional relevance. *J. Leukocyte Biol.* **2005**, *78*, 1192-1197
20. Rivers, J. R.; Ashton, J. C. The development of cannabinoid CBII receptor agonists for the treatment of central neuropathies. *Cent. Nerv. Syst. Agents Med. Chem.* **2010**, *10*, 47-64
21. Little, J. P.; Villanueva, E. B.; Klegeris, A. Therapeutic potential of cannabinoids in the treatment of neuroinflammation associated with Parkinson's disease. *Mini-Rev. Med. Chem.* **2011**, *11*, 582-590
22. c.w.Biorender.
23. Concannon, R. M.; Okine, B. N.; Finn, D. P.; Dowd, E. Upregulation of the cannabinoid CB2 receptor in environmental and viral inflammation-driven rat models of Parkinson's disease. *Exp. Neurol.* **2016**, *283*, 204-212
24. Aso, E.; Ferrer, I. CB2 Cannabinoid Receptor As Potential Target against Alzheimer's Disease. *Front. Neurosci.* **2016**, *10*, 243
25. Cecyre, B.; Thomas, S.; Ptito, M.; Casanova, C.; Bouchard, J. F. Evaluation of the specificity of antibodies raised against cannabinoid receptor type 2 in the mouse retina. *Naunyn Schmiedebergs Arch Pharmacol* **2014**, *387*, 175-184
26. Marchalant, Y.; Brownjohn, P. W.; Bonnet, A.; Kleffmann, T.; Ashton, J. C. Validating Antibodies to the Cannabinoid CB2 Receptor: Antibody Sensitivity Is Not Evidence of Antibody Specificity. *J. Histochem. Cytochem.* **2014**, *62*, 395-404
27. Zhang, H. Y.; Shen, H.; Jordan, C. J.; Liu, Q. R.; Gardner, E. L.; Bonci, A.; Xi, Z. X. CB2 receptor antibody signal specificity: correlations with the use of partial CB2-knockout mice and anti-rat CB2 receptor antibodies. *Acta Pharmacol. Sin.* **2019**, *40*, 398-409
28. Brownjohn, P. W.; Ashton, J. C. Spinal cannabinoid CB2 receptors as a target for neuropathic pain: an investigation using chronic constriction injury. *Neuroscience* **2012**, *203*, 180-193
29. Gazzi, T.; Brennecke, B.; Atz, K.; Korn, C.; Sykes, D.; Forn-Cuni, G.; Pfaff, P.; Sarott, R. C.; Westphal, M. V.; Mostinski, Y.; Mach, L.; Wasinska-Kalwa, M.; Weise, M.; Hoare, B. L.; Miljuš, T.; Mexi, M.; Roth, N.; Koers, E. J.; Guba, W.; Alker, A.; Rufer, A. C.; Kusznir, E. A.; Huber, S.; Raposo, C.; Zirwes, E. A.; Osterwald, A.; Pavlovic, A.; Moes, S.; Beck, J.; Nettekoven, M.; Benito-Cuesta, I.; Grande, T.; Drawnel, F.; Widmer, G.; Holzer, D.; van der Wel, T.; Mandhair, H.; Honer, M.; Fingerle, J.; Scheffel, J.; Broichhagen, J.; Gawrisch, K.; Romero, J.; Hillard, C. J.; Varga, Z. V.; van der Stelt, M.; Pacher, P.; Gertsch, J.; Ullmer, C.; McCormick, P. J.; Oddi, S.; Spaink, H. P.; Maccarrone, M.; Veprintsev, D. B.; Carreira, E. M.; Grether, U.; Nazaré, M. Detection of cannabinoid receptor type 2 in native cells and zebrafish with a highly potent, cell-permeable fluorescent probe. *Chem. Sci.* **2022**, *13*, 5539-5545
30. Sarott, R. C.; Westphal, M. V.; Pfaff, P.; Korn, C.; Sykes, D. A.; Gazzi, T.; Brennecke, B.; Atz, K.; Weise, M.; Mostinski, Y.; Hompluem, P.; Koers, E.; Miljus, T.; Roth, N. J.; Asmelash, H.; Vong, M. C.; Piovesan, J.; Guba, W.; Rufer, A. C.; Kusznir, E. A.; Huber, S.; Raposo, C.; Zirwes, E. A.; Osterwald, A.; Pavlovic, A.; Moes, S.; Beck, J.; Benito-Cuesta, I.; Grande, T.; Ruiz de Marti, N. E. S.; Yeliseev, A.; Drawnel, F.; Widmer, G.; Holzer, D.; van der Wel, T.; Mandhair, H.; Yuan, C. Y.; Drobyski, W. R.; Saroz, Y.; Grimsey, N.; Honer, M.; Fingerle, J.; Gawrisch, K.; Romero, J.; Hillard, C. J.; Varga, Z. V.; van der Stelt, M.; Pacher, P.; Gertsch, J.; McCormick, P. J.; Ullmer, C.; Oddi, S.; Maccarrone, M.; Veprintsev, D. B.; Nazare, M.; Grether, U.; Carreira, E. M. Development of High-Specificity Fluorescent Probes to Enable Cannabinoid Type 2 Receptor Studies in Living Cells. *J. Am. Chem. Soc.* **2020**, *142*, 16953-16964
31. Cooper, A.; Singh, S.; Hook, S.; Tyndall, J. D. A.; Vernall, A. J. Chemical Tools for Studying Lipid-Binding Class A G Protein-Coupled Receptors. *Pharmacol. Rev.* **2017**, *69*, 316-353
32. Chen, D. J.; Gao, M.; Gao, F. F.; Su, Q. X.; Wu, J. Brain cannabinoid receptor 2: expression, function and modulation. *Acta Pharmacol. Sin.* **2017**, *38*, 312-316
33. Grimsey, N. L.; Goodfellow, C. E.; Dragunow, M.; Glass, M. Cannabinoid receptor 2 undergoes Rab5-mediated internalization and recycles via a Rab11-dependent pathway. *Biochim. Biophys. Acta* **2011**, *1813*, 1554-1560
34. Wang, L.; Frei, M. S.; Salim, A.; Johnsson, K. Small-Molecule Fluorescent Probes for Live-Cell Super-Resolution Microscopy. *J. Am. Chem. Soc.* **2019**, *141*, 2770-2781
35. Westphal, M. V.; Sarott, R. C.; Zirwes, E. A.; Osterwald, A.; Guba, W.; Ullmer, C.; Grether, U.; Carreira, E. M. Highly Selective, Amine-Derived Cannabinoid Receptor 2 Probes. *Chem. Eur. J.* **2020**, *26*, 1380-1387
36. Hayashi, T.; Hamachi, I. Traceless affinity labeling of endogenous proteins for functional analysis in living cells. *Acc. Chem. Res.* **2012**, *45*, 1460-1469
37. Tamura, T.; Hamachi, I. Chemistry for Covalent Modification of Endogenous/Native Proteins: From Test Tubes to Complex Biological Systems. *J. Am. Chem. Soc.* **2019**, *141*, 2782-2799
38. Wold, F. Affinity labeling-an overview. *Methods Enzymol.* **1977**, *46*, 3-14

39. Wakayama, S.; Kiyonaka, S.; Arai, I.; Kakegawa, W.; Matsuda, S.; Ibata, K.; Nemoto, Y. L.; Kusumi, A.; Yuzaki, M.; Hamachi, I. Chemical labelling for visualizing native AMPA receptors in live neurons. *Nat. Commun.* **2017**, *8*, 14850-14864
40. Arttamangkul, S.; Plazek, A.; Platt, E. J.; Jin, H.; Murray, T. F.; Birdsong, W. T.; Rice, K. C.; Farrens, D. L.; Williams, J. T. Visualizing endogenous opioid receptors in living neurons using ligand-directed chemistry. *eLife* **2019**, *8*,
41. Fujishima, S. H.; Yasui, R.; Miki, T.; Ojida, A.; Hamachi, I. Ligand-directed acyl imidazole chemistry for labeling of membrane-bound proteins on live cells. *J. Am. Chem. Soc.* **2012**, *134*, 3961-3964
42. Hughes, C. C.; Yang, Y. L.; Liu, W. T.; Dorrestein, P. C.; La Clair, J. J.; Fenical, W. Marinopyrrole A target elucidation by acyl dye transfer. *J. Am. Chem. Soc.* **2009**, *131*, 12094-12096
43. Jing, C.; Cornish, V. W. A fluorogenic TMP-tag for high signal-to-background intracellular live cell imaging. *ACS Chem. Biol.* **2013**, *8*, 1704-1712
44. Kojima, H.; Fujita, Y.; Takeuchi, R.; Ikebe, Y.; Ohashi, N.; Yamamoto, K.; Itoh, T. Cyclization Reaction-Based Turn-on Probe for Covalent Labeling of Target Proteins. *Cell Chem. Biol.* **2020**, *27*, 334-349
45. Masuya, T.; Murai, M.; Ifuku, K.; Morisaka, H.; Miyoshi, H. Site-specific chemical labeling of mitochondrial respiratory complex I through ligand-directed tosylate chemistry. *Biochemistry* **2014**, *53*, 2307-2317
46. Takaoka, Y.; Nishikawa, Y.; Hashimoto, Y.; Sasaki, K.; Hamachi, I. Ligand-directed dibromophenyl benzoate chemistry for rapid and selective acylation of intracellular natural proteins. *Chem. Sci.* **2015**, *6*, 3217-3224
47. Tamura, T.; Tsukiji, S.; Hamachi, I. Native FKBP12 engineering by ligand-directed tosyl chemistry: labeling properties and application to photo-cross-linking of protein complexes in vitro and in living cells. *J. Am. Chem. Soc.* **2012**, *134*, 2216-2226
48. Yamaura, K.; Kiyonaka, S.; Numata, T.; Inoue, R.; Hamachi, I. Discovery of allosteric modulators for GABAA receptors by ligand-directed chemistry. *Nat. Chem. Biol.* **2016**, *12*, 822-830
49. Zhang, X.; Jiang, L.; Huang, K.; Fang, C.; Li, J.; Yang, J.; Li, H.; Ruan, X.; Wang, P.; Mo, M.; Wu, P.; Xu, Y.; Peng, C.; Uesugi, M.; Ye, D.; Yu, F. X.; Zhou, L. Site-Selective Phosphoglycerate Mutase 1 Acetylation by a Small Molecule. *ACS Chem. Biol.* **2020**, *15*, 632-639
50. Tamura, T.; Song, Z.; Amaike, K.; Lee, S.; Yin, S.; Kiyonaka, S.; Hamachi, I. Affinity-Guided Oxime Chemistry for Selective Protein Acylation in Live Tissue Systems. *J. Am. Chem. Soc.* **2017**, *139*, 14181-14191
51. Tsukiji, S.; Miyagawa, M.; Takaoka, Y.; Tamura, T.; Hamachi, I. Ligand-directed tosyl chemistry for protein labeling in vivo. *Nat. Chem. Biol.* **2009**, *5*, 341-343
52. Matsuo, K.; Nishikawa, Y.; Masuda, M.; Hamachi, I. Live-Cell Protein Sulfonylation Based on Proximity-driven N-Sulfonyl Pyridone Chemistry. *Angew. Chem., Int. Ed.* **2018**, *57*, 659-662
53. Tamura, T.; Ueda, T.; Goto, T.; Tsukidate, T.; Shapira, Y.; Nishikawa, Y.; Fujisawa, A.; Hamachi, I. Rapid labelling and covalent inhibition of intracellular native proteins using ligand-directed *N*-acyl-*N*-alkyl sulfonamide. *Nat. Commun.* **2018**, *9*, 1870-1882
54. Ireland, R. E. *Organic Synthesis*; Prentice-Hall, 1969.
55. Crispino, G. A.; Ho, P. T.; Sharpless, K. B. Selective perhydroxylation of squalene: taming the arithmetic demon. *Science* **1993**, *259*, 64-66
56. Mortensen, M. R.; Skovsgaard, M. B.; Gothelf, K. V. Considerations on Probe Design for Affinity-Guided Protein Conjugation. *ChemBioChem* **2019**, *20*, 2711-2728
57. Shiraiwa, K.; Cheng, R.; Nonaka, H.; Tamura, T.; Hamachi, I. Chemical Tools for Endogenous Protein Labeling and Profiling. *Cell Chem. Biol.* **2020**, *27*, 970-985
58. Vernall, A. J.; Stoddart, L. A.; Briddon, S. J.; Ng, H. W.; Laughton, C. A.; Doughty, S. W.; Hill, S. J.; Kellam, B. Conversion of a non-selective adenosine receptor antagonist into A3-selective high affinity fluorescent probes using peptide-based linkers. *Org. Biomol. Chem.* **2013**, *11*, 5673-5682
59. Sexton, M.; Woodruff, G.; Horne, E. A.; Lin, Y. H.; Muccioli, G. G.; Bai, M.; Stern, E.; Bornhop, D. J.; Stella, N. NIR-mbc94, a fluorescent ligand that binds to endogenous CB(2) receptors and is amenable to high-throughput screening. *Chem. Biol.* **2011**, *18*, 563-568
60. Cooper, A. G.; MacDonald, C.; Glass, M.; Hook, S.; Tyndall, J. D. A.; Vernall, A. J. Alkyl indole-based cannabinoid type 2 receptor tools: Exploration of linker and fluorophore attachment. *Eur. J. Med. Chem.* **2018**, *145*, 770-789
61. Baker, J. G.; Middleton, R.; Adams, L.; May, L. T.; Briddon, S. J.; Kellam, B.; Hill, S. J. Influence of fluorophore and linker composition on the pharmacology of fluorescent adenosine A1 receptor ligands. *Br. J. Pharmacol.* **2010**, *159*, 772-786
62. Pettinger, J.; Jones, K.; Cheeseman, M. D. Lysine-Targeting Covalent Inhibitors. *Angew. Chem. Int. Ed.* **2017**, *56*, 15200-15209
63. Yamaguchi, T.; Asanuma, M.; Nakanishi, S.; Saito, Y.; Okazaki, M.; Dodo, K.; Sodeoka, M. Turn-ON fluorescent affinity labeling using a small bifunctional *O*-nitrobenzoxadiazole unit. *Chem. Sci.* **2014**, *5*, 1021-1029
64. Uchiyama, S.; Takehira, K.; Kohtani, S.; Imai, K.; Nakagaki, R.; Tobita, S.; Santa, T. Fluorescence on–off switching mechanism of benzofurazans. *Org. Biomol. Chem.* **2003**, *1*, 1067-1072
65. Uchiyama, S.; Santa, T.; Fukushima, T.; Homma, H.; Imai, K. Effects of the substituent groups at the 4- and 7-positions on the fluorescence characteristics of benzofurazan compounds. *J. Chem. Soc., Perkin Trans. 2* **1998**, 2165-2174
66. Xing, C.; Zhuang, Y.; Xu, T. H.; Feng, Z.; Zhou, X. E.; Chen, M.; Wang, L.; Meng, X.; Xue, Y.; Wang, J.; Liu, H.; McGuire, T. F.; Zhao, G.; Melcher, K.; Zhang, C.; Xu, H. E.; Xie, X. Q. Cryo-EM Structure of the Human Cannabinoid Receptor CB2-Gi Signaling Complex. *Cell* **2020**, *180*, 645-654
67. Xue, D.; Ye, L.; Zheng, J.; Wu, Y.; Zhang, X.; Xu, Y.; Li, T.; Stevens, R. C.; Xu, F.; Zhuang, M.; Zhao, S.; Zhao, F.; Tao, H. The structure-based traceless specific fluorescence labeling of the smoothened receptor. *Org. Biomol. Chem.* **2019**, *17*, 6136-6142
68. Probes featuring linker lengths of 5, 15, 20, and 25 atoms were also docked, however, such linkers appeared either too short or unnecessarily long and flexible.
69. Li, X.; Hua, T.; Vemuri, K.; Ho, J. H.; Wu, Y.; Wu, L.; Popov, P.; Benchama, O.; Zvonok, N.; Locke, K.; Qu, L.; Han, G. W.; Iyer, M. R.; Cinar, R.; Coffey, N. J.; Wang, J.; Wu, M.; Katritch, V.; Zhao, S.; Kunos, G.; Bohn, L. M.; Makriyannis, A.; Stevens, R. C.; Liu, Z. J. Crystal Structure of the Human Cannabinoid Receptor CB2. *Cell* **2019**, *176*, 459-467
70. Jo, S.; Kim, T.; Iyer, V. G.; Im, W. CHARMM-GUI: a web-based graphical user interface for CHARMM. *J. Comput. Chem.* **2008**, *29*, 1859-1865
71. Wu, E. L.; Cheng, X.; Jo, S.; Rui, H.; Song, K. C.; Davila-Contreras, E. M.; Qi, Y.; Lee, J.; Monje-Galvan, V.; Venable, R. M.; Klauda, J. B.; Im, W. CHARMM-GUI Membrane Builder toward realistic biological membrane simulations. *J. Comput. Chem.* **2014**, *35*, 1997-2004
72. Case, D. A.; Aktulga, H. M.; Belfon, K.; Ben-Shalom, I. Y.; Berryman, J. T.; Brozell, S. R.; Cerutti, D. S.; Cheatham, I., T.E.; Cisneros, G. A.; Cruzeiro, V. W. D.; Darden, T. A.; Duke, R. E.; Giambasu, G.; Gilson, M. K.; Gohlke, H.; Goetz, A. W.; Harris, R.; Izadi, S.; Izmailov, S. A.; Kasavajhala, K.; Kaymak, M. C.; King, E.; Kovalenko, A.; Kurtzman, T.; Lee, T. S.; LeGrand, S.; Li, P.; Lin, C.; Liu, J.; Luchko, T.; Luo, R.; Machado, M.; Man, V.; Manathunga, M.; Merz, K. M.; Miao, Y.; Mikhailovskii, O.; Monard, G.; Nguyen, H.; O'Hearn, K. A.; Onufriev, A.; Pan, F.; Pantano, S.; Qi, R.; Rahnamoun, A.; Roe, D. R.; Roitberg, A.; Sagui, C.; Schott-Verdugo, S.; Shajan, A.; Shen, J.; Simmerling, C. L.; Skrynnikov, N. R.; Smith, J.; Swails, J.; Walker, R. C.; Wang, J.; Wang, J.; Wei, H.; Wolf, R. M.; Wu, X.; Xiong, Y.; Xue, Y.; York, D. M.; Zhao, S.; Kollman, P. A. *Amber* **2022**, *University of California, San Francisco,*
73. Hua, T.; Li, X.; Wu, L.; Iliopoulos-Tsoutsouvas, C.; Wang, Y.; Wu, M.; Shen, L.; Brust, C. A.; Nikas, S. P.; Song, F.; Song, X.; Yuan, S.; Sun, Q.; Wu, Y.; Jiang, S.; Grim, T. W.; Benchama, O.; Stahl, E. L.; Zvonok, N.; Zhao, S.; Bohn, L. M.; Makriyannis, A.; Liu, Z. J. Activation and Signaling

Mechanism Revealed by Cannabinoid Receptor-Gi Complex Structures. *Cell* **2020**, *180*, 655-665

74. Li, X.; Chang, H.; Bouma, J.; de Paus, L. V.; Mukhopadhyay, P.; Paloczi, J.; Mustafa, M.; van der Horst, C.; Kumar, S. S.; Wu, L.; Yu, Y.; van den Berg, R.; Janssen, A. P. A.; Lichtman, A.; Liu, Z. J.; Pacher, P.; van der Stelt, M.; Heitman, L. H.; Hua, T. Structural basis of selective cannabinoid CB(2) receptor activation. *Nat. Commun.* **2023**, *14*, 1447-1463

75. Reddi, R. N.; Rogel, A.; Resnick, E.; Gabizon, R.; Prasad, P. K.; Gurwicz, N.; Barr, H.; Shulman, Z.; London, N. Site-Specific Labeling of Endogenous Proteins Using CoLDR Chemistry. *J. Am. Chem. Soc.* **2021**, *143*, 20095-20108

76. Tamura, T.; Kioi, Y.; Miki, T.; Tsukiji, S.; Hamachi, I. Fluorophore labeling of native FKBP12 by ligand-directed tosyl chemistry allows detection of its molecular interactions *in vitro* and in living cells. *J. Am. Chem. Soc.* **2013**, *135*, 6782-6785

77. Stoddart, L. A.; Kindon, N. D.; Otun, O.; Harwood, C. R.; Patera, F.; Veprintsev, D. B.; Woolard, J.; Briddon, S. J.; Franks, H. A.; Hill, S. J.; Kellam, B. Ligand-directed covalent labelling of a GPCR with a fluorescent tag in live cells. *Commun. Biol.* **2020**, *3*, 722-731

78. Although we demonstrate a complete transfer of NBD to $CB_2R$ in the case of **2b**, *vide infra*, in principle the addition of SR-144,528 can also displace unreacted *O*-NBD probes.

79. Soethoudt, M.; Grether, U.; Fingerle, J.; Grim, T. W.; Fezza, F.; de Petrocellis, L.; Ullmer, C.; Rothenhausler, B.; Perret, C.; van Gils, N.; Finlay, D.; MacDonald, C.; Chicca, A.; Gens, M. D.; Stuart, J.; de Vries, H.; Mastrangelo, N.; Xia, L.; Alachouzos, G.; Baggelaar, M. P.; Martella, A.; Mock, E. D.; Deng, H.; Heitman, L. H.; Connor, M.; Di Marzo, V.; Gertsch, J.; Lichtman, A. H.; Maccarrone, M.; Pacher, P.; Glass, M.; van der Stelt, M. Cannabinoid CB2 receptor ligand profiling reveals biased signalling and off-target activity. *Nat. Commun.* **2017**, *8*, 13958-13972

80. RO7663417 is a proprietary $CB_2R$-selective high affinity probe functionalized with Alexa647 fluorophore developed at F. Hoffmann-La Roche whose structure will be disclosed shortly.

81. Benson, D. M.; Bryan, J.; Plant, A. L.; Gotto, A. M., Jr.; Smith, L. C. Digital imaging fluorescence microscopy: spatial heterogeneity of photobleaching rate constants in individual cells. *J. Cell Biol.* **1985**, *100*, 1309-1323

82. Thimaradka, V.; Hoon Oh, J.; Heroven, C.; Radu Aricescu, A.; Yuzaki, M.; Tamura, T.; Hamachi, I. Site-specific covalent labeling of His-tag fused proteins with N-acyl-N-alkyl sulfonamide reagent. *Bioorg. Med. Chem.* **2021**, *30*, 115947-115953

83. Tivon, Y.; Falcone, G.; Deiters, A. Protein Labeling and Crosslinking by Covalent Aptamers. *Angew. Chem. Int. Ed.* **2021**, *60*, 15899-15904

84. Ueda, T.; Tamura, T.; Hamachi, I. Development of a Cell-Based Ligand-Screening System for Identifying Hsp90 Inhibitors. *Biochemistry* **2020**, *59*, 179-182

85. Ueda, T.; Tamura, T.; Kawano, M.; Shiono, K.; Hobor, F.; Wilson, A. J.; Hamachi, I. Enhanced Suppression of a Protein-Protein Interaction in Cells Using Small-Molecule Covalent Inhibitors Based on an N-Acyl-N-alkyl Sulfonamide Warhead. *J. Am. Chem. Soc.* **2021**, *143*, 4766-4774

86. Teng, M.; Jiang, J.; Ficarro, S. B.; Seo, H. S.; Bae, J. H.; Donovan, K. A.; Fischer, E. S.; Zhang, T.; Dhe-Paganon, S.; Marto, J. A.; Gray, N. S. Exploring Ligand-Directed N-Acyl-N-alkylsulfonamide-Based Acylation Chemistry for Potential Targeted Degrader Development. *ACS Med. Chem. Lett.* **2021**, *12*, 1302-1307

87. Atwood, B. K.; Lopez, J.; Wager-Miller, J.; Mackie, K.; Straiker, A. Expression of G protein-coupled receptors and related proteins in HEK293, AtT20, BV2, and N18 cell lines as revealed by microarray analysis. *BMC Genomics* **2011**, *12*, 14. HEK293 wild-type cells serve as a suitable negative control as they do not express $CB_2R$ as judged by RNAseq.

88. Miljuš, T.; Heydenreich, F. M.; Gazzi, T.; Kimbara, A.; Roger-Evans, M.; Nettekoven, M.; Zirwes, E.; Osterwald, A.; Rufer, A. C.; Ullmer, Ch.; Guba, W.; Le Gouill, Ch.; Fingerle, J.; Nazaré, M.; Grether, U.; Bouvier, M.; Veprintsev, D. Diverse chemotypes drive biased signaling by cannabinoid receptors. **2020** bioRxiv doi: 10.1101/2020.11.09.375162. $CB_2R$-mediated signaling was not detected from non-transfected cells using BRET-based biosensor assays.

89. Soethoudt, M.; Stolze, S. C.; Westphal, M. V.; van Stralen, L.; Martella, A.; van Rooden, E. J.; Guba, W.; Varga, Z. V.; Deng, H.; van Kasteren, S. I.; Grether, U.; AP, I. J.; Pacher, P.; Carreira, E. M.; Overkleeft, H. S.; Ioan-Facsinay, A.; Heitman, L. H.; van der Stelt, M. Selective Photoaffinity Probe That Enables Assessment of Cannabinoid CB2 Receptor Expression and Ligand Engagement in Human Cells. *J. Am. Chem. Soc.* **2018**, *140*, 6067-6075

90. Barteneva, N. S.; Vorobjev, I. A. *Imaging Flow Cytometry*; Humana New York, 2016.

91. Cells are incubated with LDC probes for 2 hours and can transfer their cargo when transiently bound to $CB_2R$. Subsequently, when the ligand is outcompeted by SR-144,528 the MFI does not decrease as the fluorophore was covalently transferred to $CB_2R$.

92. Henn, A.; Lund, S.; Hedtjarn, M.; Schrattenholz, A.; Porzgen, P.; Leist, M. The suitability of BV2 cells as alternative model system for primary microglia cultures or for animal experiments examining brain inflammation. *ALTEX* **2009**, *26*, 83-94

93. Stansley, B.; Post, J.; Hensley, K. A comparative review of cell culture systems for the study of microglial biology in Alzheimer's disease. *J. Neuroinflammation* **2012**, *9*, 115-123

94. Yao, K.; Zu, H. B. Microglial polarization: novel therapeutic mechanism against Alzheimer's disease. *Inflammopharmacology* **2020**, *28*, 95-110

95. Franklin, A.; Stella, N. Arachidonylcyclopropylamide increases microglial cell migration through cannabinoid CB2 and abnormal-cannabidiol-sensitive receptors. *Eur. J. Pharmacol.* **2003**, *474*, 195-198

96. Han, Q. W.; Shao, Q. H.; Wang, X. T.; Ma, K. L.; Chen, N. H.; Yuan, Y. H. CB2 receptor activation inhibits the phagocytic function of microglia through activating ERK/AKT-Nurr1 signal pathways. *Acta Pharmacol. Sin.* **2022**, *43*, 2253-2266

97. Iwamura, H.; Suzuki, H.; Ueda, Y.; Kaya, T.; Inaba, T. In vitro and in vivo pharmacological characterization of JTE-907, a novel selective ligand for cannabinoid CB2 receptor. *J. Pharmacol. Exp. Ther.* **2001**, *296*, 420-425

98. Singh, S.; Oyagawa, C. R. M.; Macdonald, C.; Grimsey, N. L.; Glass, M.; Vernall, A. J. Chromenopyrazole-based High Affinity, Selective Fluorescent Ligands for Cannabinoid Type 2 Receptor. *ACS Med. Chem. Lett.* **2019**, *10*, 209-214. The single inverse agonist probe, in a series of agonist probes featuring the same ligand, owes its functional profile to a specific linker length and fluorophore.

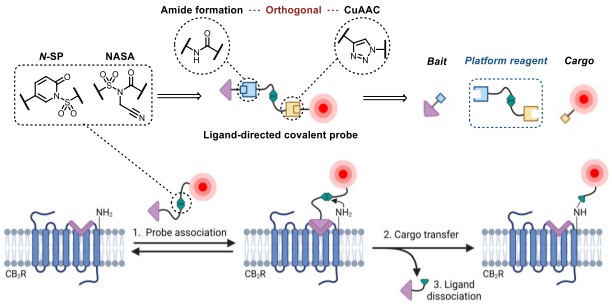
Amide formation --- Orthogonal --- CuAAC
N-SP
NASA
Bait
Platform reagent
Cargo
Ligand-directed covalent probe
NH2
1. Probe association
2. Cargo transfer
3. Ligand dissociation
CB2R
NH